Plant-minerals-water interactions: an investigation on *Juncus acutus* exposed to different Zn sources

Daniela Medas[a,*], Carlo Meneghini[b], Claudia Pusceddu[a], Ilaria Carlomagno[c], Giuliana Aquilanti[c], Elisabetta Dore[a], Vittorio Murgia[d], Francesca Podda[a], Valentina Rimondi[e,f], Salvatore Vacca[a], Richard B. Wanty[g], Giovanni De Giudici[a]

[a]Department of Chemical and Geological Science, University of Cagliari, Cagliari, Italy – dmedas@unica.it, clau.pux@libero.it, elisabetta.dore@unica.it, fpodda@unica.it, salvacca@unica.it, gbgiudic@unica.it

[b]Department of Sciences, University of Roma Tre, Rome, Italy - carlo.meneghini@uniroma3.it

[c]Elettra-Sincrotrone Trieste, Basovizza, Trieste, Italy - ilaria.carlomagno@elettra.eu, giuliana.aquilanti@elettra.eu

[d]Soc. Agr. Sgaravatti Land Cons. Arl, Cagliari, Italy – vittorio.murgia@sgaravattigroup.it

[e]Department of Earth Sciences, University of Florence, Florence, Italy - valentina.rimondi@unifi.it

[f]CNR—Institute of Geosciences and Earth Resources, Florence, Italy - valentina.rimondi@unifi.it

[g]Colorado School of Mines, Department of Geology and Geological Engineering, Golden, CO 80401 USA - rwanty@mines.edu

*dmedas@unica.it

Abstract

Juncus acutus has been proposed as a species apt for the design of phytoremediation plans. This research aimed to investigate the role played by rhizosphere minerals and water composition on Zn transformations and dynamics in the rhizosphere-plant system of *J. acutus* exposed to different Zn sources. Rhizobox experiments were conducted using three different growing substrates (Zn from 137 to 20400 mg/kg), and two irrigation lines (Zn 0.05 and 180 mg/l). The plant growth was affected by the substrate type, and the Zn content in the water did not significantly influence the plant height for a specific substrate. *J. acutus* accumulated Zn mainly in roots (up to 10000 mg/kg dw), and the metal supply by the water led to variable increases in the total Zn concentration in the vegetal tissues, and different Zn distributions both controlled by the rhizosphere mineral composition. Different Zn complexation mechanisms were observed, mainly driven by cysteine and citrate compounds whose amount increased linearly with Zn content in water but differently for the investigated systems.

Our findings contribute to gain a more complete picture of the Zn pathway in the rhizosphere-plant system, highlighting the critical role played by the rhizosphere minerals, and providing fundamentals for the development of effective phytoremediation plans.

Keywords

Pollutants; metal speciation; rhizosphere minerals; XANES

Introduction

Trace metals occur naturally in rocks, soils and waters, but higher quantities are being released into the environment by anthropogenic activities (Kwon et al., 2022; Zovko and Romic, 2011), such as industrial, mining, shipping and agricultural

activities. Metals cannot be synthesized or degraded by biological or chemical processes, although their chemical forms (e.g., oxidation state, complexation) can change. They can be chemically very reactive in the environment, leading to their mobility and bioavailability to living organisms with potential detrimental effects (Briffa et al. 2020, and references therein). As a result, there is a great necessity for efficient tools to prevent metal dispersion (Wang et al., 2021; Zhou et al., 2020; Zoumis et al., 2000) and transfer to the food chain. Phytostabilization is an especially suitable method in highly polluted areas (Frérot et al., 2006; Pérez-Esteban et al., 2014; Salt et al., 1995). It exploits plant cover to prevent pollutants from spreading by erosion, water infiltration, leaching and from toxic dust dispersal by wind (Frérot et al. 2006, and references therein). *Juncus acutus* L. has evolved adaptive mechanisms, in particular metal tolerance (Fancello et al., 2019; Freitas et al., 2009; Landsberger et al., 2010; Santos et al., 2014; Stefani et al., 1991; Syranidou et al., 2017a), allowing it to thrive on mine soils (Syranidou et al., 2017a). As with other macrophytes (Marchand et al., 2010), *J. acutus* plays a significant role in the riverbed processes, reducing metal mobility by limiting erosive processes, promoting the sedimentation of suspended particles, providing organic matter for bacterial metabolism, and potential sites for metal sorption. Also, it was observed (Dore et al., 2020) that *J. acutus* can favor the formation of authigenic sulfides (mainly FeS_2) in the hyporheic zone. These capabilities render this plant species an effective phytostabilizer, useful for revegetation of Zn-contaminated lands (Mateos-Naranjo et al., 2014; Syranidou et al., 2017a), and as a tool for wetland restoration projects around the world (Aydın Temel et al., 2018; Santos et al., 2014; Sparks et al., 2013; Zaimoglu, 2006). Several experimental studies were conducted on *J. acutus* grown under different Zn concentrations. Mateos-Naranjo et al. (2014) investigated the effect of Zn (from 0 to 100 mM) on the growth, photosynthetic apparatus, and nutrient uptake. *J. acutus* showed high tolerance to Zn-induced stress. The integrity and functionality of the photosynthetic apparatus were unaffected even at Zn concentrations (560 mg/kg in stems) greater than toxicity thresholds recorded for plants (100-500 mg/kg) (Kabata-Pendias, 2000). Authors reported that Zn tolerance is related to the plants' capacity to accumulate Zn in roots (up to 2500 mg/kg in their study), avoiding its transport to stems, possibly by the development of mechanisms such as compartmentalization (Caldelas and Weiss, 2017). Likewise, Santos et al. (2014) found that *J. acutus* can tolerate exogenous Zn concentrations up to 60 mM (in growth medium). Zinc concentrations in seedlings germinated in the presence of high Zn concentrations, were above the described upper toxic levels for higher plants (100-500 mg/kg), confirming the results in Mateos-Naranjo et al. (2014). The damage produced during the metal uptake was efficiently overcome by dissipating the excessive cellular redox potential accumulated, essentially due to Zn incorporation into the chlorophyll molecule (Santos et al., 2014). Mateos-Naranjo et al. (2018) designed a factorial greenhouse experiment to assess the effect of NaCl supply (0 and 85 mM NaCl) on the growth, photosynthetic physiology and ion concentrations of tissues of plants exposed to 0, 30 and 100 mM Zn. They found that NaCl supplementation, at concentrations representative of estuarine environments, alleviates the effects of Zn toxicity on growth because of a reduction in Zn tissue concentrations, and protective effects during the photosynthetic pathway.

The increasing number of literature studies (Alam et al., 2022; Christofilopoulos et al., 2016; Duarte et al., 2021; Syranidou et al., 2017b, 2017a, 2016) demonstrates the interest and the need for an in-depth knowledge of metal geo-biotransformation in the rhizosphere-plant system of *J. acutus*. Moreover, to the best of our knowledge, previous researches specifically aimed at investigating the relationship between Zn source and Zn complexation in plants (da Cruz et al., 2019; Doolette et al., 2018; Montanha et al., 2020; Wang et al., 2013) are limited and need further investigations. Our work delves into the understanding of Zn transformations and dynamics during rhizosphere-plant interactions when plants are exposed to different metal sources. For this purpose, we selected *J. acutus*, a plant species characterized by i) a sub-cosmopolitan distribution, ii) a wide ecological range, iii) a high dispersion potential, due to its abundant seed production and high germination rate, iv) a great tolerance to high concentration of metals, sulphates and chlorides, and

to hydric stress during the dry summer season, and v) a high potential for phytostabilization projects (Brown and Bettink, 2006; Lombardo, 1982; López-Juambeltz et al., 2020; Mateos-Naranjo et al., 2018, 2014). These properties render *J. acutus* and its interactions with the environment of great relevance for a multidisciplinary and global audience.

Previous studies (Medas et al., 2019) demonstrated that *J. acutus* grown in natural mining environments can optimize its adaptation in response to the mineralogy and geochemical conditions of the site. Here, we performed a rhizobox experiment (Hylander, 2002), under greenhouse conditions, to isolate the influence of rhizosphere minerals and water composition, using three different growing substrates (two polluted substrates from abandoned mining sites and an unpolluted potting soil) and two different irrigation lines (Clean Water line – Zn_{water} 0.05 mg/l; Zn-spiked Water line – Zn_{water} 180 mg/l). A multi-technique characterization was performed, combining chemical, X-ray diffraction (XRD) and X-ray absorption near edge structure (XANES) analysis to investigate Zn distribution and complexation. The aim was to reach a better understanding of the Zn pathway in the rhizosphere-plant system, and to assess the role played by the rhizosphere minerals and water composition on Zn uptake processes.

Materials and methods

Rhizobox experiment

Rhizobox experiment was performed in the greenhouse "Vivai Murgia" (Villacidro, SW Sardinia). The rhizoboxes (Fig. 1) were made up of transparent plexiglass (L x H x W = 200 x 300 x 50 mm) and were laterally covered by removable strips of dark fabric to protect the roots from light. Eighteen rhizoboxes were divided into two groups and were placed onto two wooden supports. The rhizoboxes were filled by three different substrates (3 replicates for each substrate): two different muddy mine wastes, from the Naracauli area (N39° 31.14', E8° 29.33', Naracauli substrate; Medas et al. 2013) and from the San Giorgio area (N39° 16.56', E8° 27.39', Sa Masa substrate; Bacchetta et al. 2015; De Giudici et al. 2017); the third substrate was an unpolluted substrate (potting soil). The substrates were sieved at 2 mm, and 2 kg of each substrate were mixed with 1 kg of commercial pozzolana, to improve their permeability. After mixing, each rhizobox was filled with the mixture.

To increase the chances for the plants to grow in the substrates characterized by high metal concentrations (Kothe and Büchel, 2014; Sprocati et al., 2014), plantlets of *J. acutus* were obtained from seeds collected from plants growing in the Naracauli mine-polluted area (Sprocati et al., 2014). The plantlets were grown up to 5-10 cm in potting soil (Fig. 1a), then their roots were gently cleaned from particles of the initial substrate, and plants were transferred in the rhizoboxes (Fig. 1b, c and d). Two plantlets were transplanted in each rhizobox.

Two irrigation lines were used, one with unpolluted water (Clean Water line (tap water), average Zn_{water} 0.05 mg/l, hereinafter referred to as CW), and another with polluted water (Zn-spiked Water line, Zn_{water} 180 mg/l, hereinafter referred to as ZnW). Zinc was supplied to the ZnW as $ZnSO_4 \cdot 7H_2O$. Watering was provided every 48 hours according to the seasonal conditions (max temperatures up to 45°C in August). It is worth noting that selected Zn concentration for the ZW is within the detected Zn concentrations in mine waste pore water, seepages and river waters draining several abandoned or active mining areas around the world, thus representing realistic environmental conditions (Bao et al., 2022; Cidu et al., 2011; Cidu and Biddau, 2005; Pavoni et al., 2018).

The experiment lasted 5 months, and the growth of plants was monitored monthly, measuring *J. acutus* height from the surface of the substrate to the highest part of the plant. At the end of the experiment, plants and rhizospheres (defined here as the soil portion collected within 2 mm from the roots) were collected and analysed. All triplicates, both the vegetal tissues and the rhizospheres, were mixed to have enough material to perform XRD, Zn chemical analysis and XANES

investigation. Also, white efflorescent salts were collected from the surface of the mine substrates from the two irrigation lines and investigated by XRD and XANES analysis. Table 1 shows the investigated sample names, acronyms and their description.

X-ray diffraction analysis

XRD analysis was performed on the substrates (before the rhizobox experiment), rhizospheres (after the rhizobox experiment), efflorescent salts, and on the vegetal tissues (roots and stems). Substrates and rhizospheres were air-dried and gently hand milled in an agate mortar. Plants were divided in roots and stems and each portion was gently washed in Milli-Q water to remove dust and any soil particle. Then, water on the root and stem surface was absorbed by filter paper, and samples were ground in a mortar with liquid nitrogen. For XRD analysis, we used a laboratory θ–θ equipment (Panalytical) operating at 40 kV and 40 mA with Cu K_α radiation (λ = 1.54060 Å), using the X'Celerator detector. Efflorescent salts were air-dried and lightly ground in an agate mortar. XRD analysis were performed at the MCX (Materials Characterization by X-ray diffraction) beamline (experiment number #20140061) of Elettra Synchrotron (Trieste, Italy) (Rebuffi et al., 2014), using an imaging plate detector which allows high count statistics suitable for revealing weak and/or broad diffraction peaks coming from low concentrated and/or poorly crystalline phases. The X-ray beam wavelength (λ = 0.82594 Å) and the experimental geometry were calibrated refining Si-NIST diffraction pattern. The samples were placed in thin wall borosilicate capillaries (inner diameter 0.3 mm) kept spinning during the data acquisition to ensure a randomized orientation of the crystallites in the sample. The XRD data were integrated to intensity vs 2θ using the Fit2D software (Hammersley et al., 1996). All diffraction patterns were analyzed with X'Pert HighScore Plus 2.1 (Panalytical, Almelo, The Netherlands) using the PDF-2 database (International Centre for Diffraction Data) to identify the crystallographic phases in the samples.

Zinc chemical analysis and biological indexes

For Zn determination in the solid samples, acid digestion was carried out on 0.25 g of both dried and ground substrate (before the experiment) and composite rhizosphere (after the experiment). A high-purity mixture of 2 ml of Milli-Q water (< 0.1 μS/cm), 2 ml of H_2O_2 (30% w/w, Sigma-Aldrich), 3 ml of HF (40%, Chem-Lab), and 12 ml of aqua regia (9 ml of HCl, suprapur 34–37%, Chem-Lab + 3 ml HNO_3, suprapur 67–69%, Carlo Erba) was added to the solids into microwave vessels. Plant roots and stems were carefully washed in Milli-Q water, dried in an oven at 40°C for one week, and lightly ground in an electric grinder (Ultra Centrifugal MillZM200, Retsch GmbH, Haan, Germany). Acid digestion was carried out on 0.5 g of each sample. A high-purity mixture of 2.5 ml of Milli-Q water (<0.1 μS/cm), 2 ml of H_2O_2 (30% w/w, Sigma-Aldrich), 0.5 ml of HF (40%, Chem-Lab), and 5 ml of HNO_3 (suprapur 67–69%, Carlo Erba) was added to the solids into microwave vessels. Samples were processed together with blanks and selected reference materials (NIST 2710, Montana Soil for the substrates and rhizospheres; SRM 1573a, tomato leaves for the vegetal tissues), prepared with the same mixture to evaluate the precision (< 5 %) and accuracy (< 5 %) of the digestion procedure. Acid digestion was performed by the microwave ETHOS One (Advanced Microwave Digestion System, Milestone). After cooling, the mixtures were transferred into Teflon beakers rinsing the vessels with a few ml of Milli-Q water. These mixtures were heated in a hot plate (~4 h, 100°C); following evaporation, 3 ml of concentrated HNO_3 were added three times. Finally, the mixtures were filtered (0.4 μm), and the solutions were diluted to 50 ml (substrates and rhizospheres) and 25 ml (vegetal tissues) final volume using Milli-Q water. Zinc was determined by inductively coupled plasma optical emission spectrometry (ICP-OES, ARL Fisons ICP Analyzer 3520 B). To estimate potential contaminations, the accuracy (< 5 %)

and precision (< 5 %) of trace element analysis, procedural blanks and reference solutions (SRM 1643e and EnviroMAT Drinking Water, High EP-H-3 and Low EP-L-3) were analyzed together with the samples.

Zinc uptake by plants was evaluated by three different factors: the biological concentration factor (BCF), the bioaccumulation coefficient (BAC), and the translocation factor (TF). The BCF quantifies the Zn (mg/kg) transfer from the rhizosphere (M_{rhizo}) to the roots (M_{roots}) (Fellet et al., 2007) according to Equation 1:

$$BCF = \frac{M_{roots}}{M_{rhizo}} \quad (1)$$

The BAC (Equation 2) estimates the transfer of Zn (mg/kg) from the rhizosphere (M_{rhizo}) to the epigean organs (M_{epi}) (Marchiol et al., 2013):

$$BAC = \frac{M_{epi}}{M_{rhizo}} \quad (2)$$

The TF (Equation 3) evaluates the translocation of Zn (mg/kg) from the roots (M_{roots}) to the epigean organs (M_{epi}) (Brooks, 2008):

$$TF = \frac{M_{epi}}{M_{roots}} \quad (3)$$

X-Ray Absorption Spectroscopy

Synchrotron based-techniques, such as XANES spectroscopy, are being employed increasingly in the investigation of soil-plant systems, and represent a suitable and powerful tool for unravelling the chemical speciation of metals and metalloids (Adediran et al., 2015; Chandrakasan et al., 2021; Chen et al., 2022; De Giudici et al., 2015; Fourati et al., 2020; Kopittke et al., 2017; Panfili et al., 2005; Parsons et al., 2002; Saraswat and Rai, 2011; Sarret et al., 2013; Zelano et al., 2020; Zhao et al., 2014). Zinc K-edge (9.659 keV) XANES measurements were performed at the XAFS beamline (experiment #20167045) (Di Cicco et al., 2009), and at the XRF beamline (Jark et al., 2014) at Elettra-Sincrotrone Trieste. The rhizosphere was removed from the roots, the roots were separated from the stems, and each plant portion was gently washed in Milli-Q water. Then, water on stem and root surface was absorbed by filter paper, samples were homogenized, frozen, by plunging them in isopentane cooled by liquid nitrogen, freeze-dried, ground to powder in a glovebox, and pressed into thin solid pellets. Substrates, rhizospheres and efflorescent salts were air-dried, gently hand milled in an agate mortar, mixed with PVP (polyvinyl pyrrolidone) matrix (as a function of the Zn content) and pressed in thin solid pellets. At the XAFS beamline, the Zn K-edge absorption spectra were acquired keeping the samples in vacuum; transmission geometry (using gas-filled ionization chambers, Oxford Instruments, Abingdon-on-Thames, UK), or in fluorescence geometry (using a Silicon Drift Detector AXAS-M, Ketek, Munich, Germany), were used depending on the Zn concentration. At the XRF beamline, the spectra were collected in the ultra-high vacuum end-station (Karydas et al., 2018) in transmission geometry (using the signals from a Hamamatsu Si-photodiode S3590-09 and from a Beam Monitoring System developed by the detector group of Elettra Sincrotrone Trieste), or in fluorescence geometry (using a Silicon Drift Detector XFlash 5030, Bruker Nano GmbH, Germany), depending on the Zn concentration.

Zn K-edge XAS spectra of each sample were collected at least in triplicate at different sample positions to improve the statistics and reduce artefacts due to possible Zn content inhomogeneities. Since in the soil-plant system Zn can be hosted in mineral phases (e.g. sulfides, sulphates, carbonates, etc.) and/or can be bound to organic compounds (e.g., organic acids, phytochelatins, metallothioneins, etc.) (Caldelas and Weiss, 2017; de la Fuente et al., 2018; Kopittke et al., 2017; Parsons et al., 2002; Salt et al., 1999; Saraswat and Rai, 2011; Sarret et al., 2006, 2002; Zhao et al., 2014), an ample set of Zn reference compounds (standards, Table S1) was measured or derived from previous experiments (Boi et al., 2020; Medas et al., 2018) carried out with the same set-up. The measurements of the reference compounds allowed us to reliably

compare the datasets collected on the two beamlines. Athena software (Ravel and Newville, 2005) has been used for preliminary XAS data treatment (background subtraction, normalization and averaging) and quantitative XANES analysis (linear combination analysis, LCA). The normalized XANES spectra of the reference compounds are shown in Fig. S1.

The principal component analysis (PCA) was performed by the SixPack software (Webb, 2005) to evaluate the number of statistically significant components (principal components) necessary to describe the variability of the experimental signals within the dataset (Etschmann et al., 2014). The target transform (TT) was used to select, among the reference compounds, the most suitable to be used to reproduce (LCA) the sample experimental data (Gaur and Shrivastava, 2012; Shi et al., 2008; Voegelin et al., 2005; Wang et al., 2013). The goodness of TT was evaluated looking at the SPOIL value (Gaur and Shrivastava, 2012) calculated by the SixPack software, and at the variance of the residues ($\sigma_r^2 = \frac{1}{N}\sum_i\left(\mu_{exp}^i - \mu_{TT}^i\right)^2$, the sum running over the experimental points, μ_{exp}^i and μ_{TT}^i being the experimental and target transformed points respectively). The suitable reference compounds were selected among those having minimum σ_r^2, and excellent to acceptable SPOIL values. Normalised sample spectra where then analysed by LCA by Athena (Ravel and Newville, 2005), within an energy range of −20 eV below to +30eV above the edge, selecting the suitable references identified by TT. For each sample, the combination of standards with the lowest R-factor and the lowest reduced χ^2 was selected as the most likely set of components.

Results

Plant growth and mineralogical characterization

Heights of *J. acutus* were measured monthly during the experiment and their values are reported in Fig. 2 and Table S2. Plant height was similar in all systems through the first month, but by the end of the experiment, plants from the unpolluted substrate were taller, for both the CW (29±5 cm after 5 months) and the ZnW (26±1 cm after 5 months), than plants from the polluted substrates (SMCW 17.3±0.9 cm, SMZnW 15±1 cm; NCW 12±1 cm and NZnW 11.8±0.7 cm).

Results of XRD analysis are reported in Table 2. Rhizospheres (from both the CW and ZnW) did not show any variation in mineralogical composition when compared to the corresponding initial substrate. Quartz (SiO_2, Qtz) and calcite ($CaCO_3$, Cal) were detected in all the substrates and rhizospheres, phyllosilicates (Ph) were found in the unpolluted and Naracauli samples, dolomite ($CaMg(CO_3)_2$, Dol) in Sa Masa samples, and feldspars (Fs) in the unpolluted ones. Accessory minerals were siderite ($FeCO_3$, Sid) and gypsum ($CaSO_4$, Gy) in the Naracauli samples, while smithsonite ($ZnCO_3$, Smith) and hemimorphite ($Zn_4Si_2O_7(OH)_2 \cdot H_2O$, Hem) were observed in Sa Masa samples. The main peaks of quartz were observed in all the roots, calcite in the roots from the unpolluted and Sa Masa systems, and dolomite in roots from the Sa Masa system from both the CW and the ZnW. In all roots and stems, we clearly observed the main peaks of cellulose at around 14.9°–16.5°2θ and 22.8°2 θ.

In the efflorescent salts (data not shown), we detected gypsum and hexahydrite ($MgSO_4{\cdot}6(H_2O)$, indicating production of sulphate from the oxidation of metal sulphides. Co-located with efflorescent salts, we also found quartz and phyllosilicates as mineral grains from the substrates, likely raised during the growth of efflorescence. As for the rhizospheres and the vegetal tissues, no differences in efflorescent salt mineralogy were detected between samples collected from the CW and the ZnW.

Zinc concentration and distribution

Figure 3 and Table S3 show the Zn concentrations in the investigated samples. At the beginning of the experiment, the substrates were characterized by an increasing Zn concentration in the order: U (Zn 137±4 mg/kg), N (Zn 9700±291 mg/kg) and SM (Zn 20400±612 mg/kg). As for the substrates, Zn increased from the unpolluted rhizospheres (UCW-rhizo Zn 150±5 mg/kg, UZnW-rhizo±91 Zn 3040 mg/kg) to the Naracauli (NCW-rhizo Zn 10400±312 mg/kg, NZnW-rhizo Zn 12500±375 mg/kg) and Sa Masa (SMCW-rhizo Zn 19500±585, SMZnW-rhizo Zn 20600±618 mg/kg) rhizospheres both in samples from the CW and the ZnW. Zinc contents in *J. acutus* roots and stems were affected by the Zn concentrations in the rhizospheres (correlation coefficient $\rho_{Zn\text{-}rhizo\text{-}roots}$ 0.94-0.99, $\rho_{Zn\text{-}rhizo\text{-}stems}$ 0.97-0.99), and followed the same trend (Zn concentration in Sa Masa *J. acutus* > Naracauli > unpolluted) along the two irrigation lines (Fig. 3 and Table S3).

We observed significant statistical differences (Z-test, p-value <0.01) between the Zn concentrations in samples from the two irrigation lines in all the investigated systems, except for the Sa Masa rhizosphere and Naracauli roots in which the Zn concentration changes were weaker (p-value > 0.1). The rhizosphere, roots and stems from the unpolluted group showed the highest increase in Zn concentration (1930% in the rhizosphere, 108% in the roots, and 51% in the stems) when plants were watered with the Zn-spiked water. In the Sa Masa group, the rhizosphere did not show any statistically significant Zn increase, whereas in roots and stems the metal concentration increased by 69% and 31%, respectively. For the Naracauli group, Zn increased by 20% in the rhizosphere and by 14% in the stems, while in the roots the difference was weak and not statistically significant.

Variations were also observed for the Zn accumulation and distribution as described by the indexes reported in Fig. 4 and Table S4 (BCF, Zn_{roots}/Zn_{rhizo}; BAC, Zn_{epi}/Zn_{rhizo}; TF, Zn_{epi}/Zn_{roots}). In the samples from the CW, BCF values were similar for the three systems (BCF_{CW} 0.30-0.42), whereas BAC and TF were higher for the plants grown on the unpolluted substrate (BAC_{UCW} 0.24, TF_{UCW} 0.69) than for plants grown on the contaminated substrates ($BAC_{NCW\text{-}SMCW}$ 0.04, $TF_{NCW\text{-}SMCW}$ 0.10-0.15), indicating that Zn accumulation in stems and its translocation were higher when Zn content in the rhizosphere was low (150 mg/kg). For the ZnW samples, indexes for the plants grown on the unpolluted substrate showed the most important variations, and they decreased (BCF_{UZnW} 0.04, BAC_{UZnW} 0.02, TF_{UZnW} 0.50), pointing out a lower Zn uptake and translocation than *J. acutus* plants from the CW. Specifically, the BCF for the unpolluted group reached the lowest value in comparison to the contaminated systems, whereas the Zn translocation was higher (TF_{UZnW} 0.50, TF_{NZnW} 0.10, TF_{SMZnW} 0.11), as for the CW. For the Sa Masa system, the BCF increased and showed the highest value (BCF_{SMZnW} 0.49), because of a higher Zn accumulation in roots in comparison to the other systems. On the contrary, BCF showed an inverse trend for the Naracauli group, slightly decreasing (BCF_{NZnW} 0.38). BAC and TF values for plants grown on both mine-waste-rich substrates did not depend on the Zn concentration of the irrigation water.

Zinc chemical speciation in solid samples

Molecular species of Zn in the initial substrates, rhizospheres and plant tissues from the two irrigation lines were investigated by bulk XANES analysis (Fig. 5). XANES spectral features were more structured in the substrates and rhizospheres and became smoother and broader in the roots and stems. These characteristics suggested that the local structure around Zn was more disordered in the vegetal tissues than in the substrates and rhizospheres.

The Zn K-edge XANES measured on the substrates and rhizosphere samples from the unpolluted and Naracauli systems depicted a double peak white line around 9665 eV, more pronounced in the Naracauli samples. The Zn-edge XANES of the Sa Masa substrate and rhizosphere showed a single peak white line and a broad shoulder in the post edge region (9680 eV), definitely different from the spectra measured in unpolluted and Naracauli samples. However, the XANES features

of the roots and stem samples appeared to preserve some of the Zn chemical species from the original substrates in all the experimental conditions.

To investigate the distribution of the Zn chemical species, we performed a LCA using the spectra measured on standard Zn compounds (Table S1 and Fig. S1) as references. This method is suitable to recognize and quantify the absorber phases in a multi-phase system like our samples, but it must be stressed here that due to the local sensitivity of XANES, the results of the LCA must be interpreted as chemical coordination environment similar to that of the reference compound. These phases may possess long-range order, therefore observable in the XRD analysis, or may be even amorphous thus may not correspond to a distinct phase in the sample.

Looking at the Zn K-edge XANES of the reference compounds several candidates may appear suitable for LCA (Fig. S1). To select the relevant compounds, we used the PCA and TT methods as described below. The PCA is an instrument of multivariate analysis allowing to identify the components contributing to the variability within a dataset, these are the eigenvectors of the covariance matrix. In the XANES analysis the components out of the statistical noise (principal components) can be associated to differences in the Zn-phase coordination chemistry among the spectra. The whole dataset of sample XANES spectra measured on substrates, rhizospheres, roots and stems from the different experimental conditions was treated by PCA (Table S5). The number of relevant components was evaluated considering different parameters: the factor indicator function (IND), the cumulative variance, and the eigenvalues. The IND indicator (Table S5) suggested that nine major spectral contributions could satisfactorily reproduce our experimental spectra, but we found the first seven components accounting for 99% of the total variance of the XANES dataset, therefore we have considered a maximum of seven reference components that should be sufficient to describe the variability of our dataset, above the noise. The eigenvalues of the covariance matrix (Fig. S2) supported our approach. Indeed, the scree plot (from the second component) shows two breaks at 3 and 7 components followed by a plateau. The overestimation of the number of components by the IND indicator could be due to some larger noise in some of the experimental spectra (Manceau et al., 2014), in particular for the spectra measured on stems and those from the unpolluted group which were characterized by low Zn concentrations (Table S3), providing a weak and noisy Zn K-edge XANES signal.

Suitable references for the LCA were identified using the TT analysis, evaluating the goodness of TT by the SPOIL value (Table S6). We selected, as potential candidates, reference compounds whose TT was characterized by a SPOIL value lower than 4.5 (limit for acceptable candidates). The relative amount of Zn species was evaluated by LCA (Fig. 6 and Table S7). The fit quality was estimated by the R-factor and reduced χ^2, a new component was considered statistically significative and added to the LCA fit when the R-factor decreased by at least 10%. LCA allowed us to identify seven different coordination environments: i) octahedral Zn (ZnO_6) in smithsonite, ii) octahedral Zn (ZnO_6) in layered double hydroxides (Zn-Al-LDH), iii) tetrahedral Zn (ZnO_4) in hemimorphite, iv) tetrahedral Zn (ZnO_4) in Zn phosphate, v) sorbed tetrahedral Zn on hydroxyapatite, vi) tetrahedral Zn (ZnS_4) in Zn cysteine, and vii) octahedral Zn (ZnO_6) complexed to citrate. It is worth noting that reference compounds that gave the best fits were those characterized by good-acceptable SPOIL values and by the lowest residual variance (<0.0002, Table S6), and their number (seven) supported the results of PCA analysis (Table S5 and Fig. S2).

In all the substrates, Zn was present in a chemical environment like that of octahedral Zn (ZnO_6) in layered minerals (Zn-Al-LDH 14-34%). Sorbed tetrahedral Zn was detected in U and N, with the highest content in the U sample (62%). In SM, relevant concentrations of tetrahedral Zn like that in hemimorphite (33%) and octahedral Zn like that in smithsonite (29%) were found, according to XRD analysis (Table 2). Tetrahedrally coordinated Zn like that in hemimorphite was also detected in N (47%). In this sample crystalline hemimorphite was not revealed by XRD but it could be present below the detection limit of 1% by volume as hemimorphite was a typical ore mineral in the abandoned mine of Naracauli (Boni et

al., 2003). Moreover, a local hemimorphite-like Zn coordination could be present as amorphous phase. A portion of Zn was also found to be octahedrally bound as in Zn citrate in U and SM. LCA results explained the differences observed between the XANES spectral features of U/N and SM samples. Indeed, the broad shoulder in the post edge region (9680 eV) of SM was due to the presence of smithsonite, whereas the double peak white line around 9665 eV originated from the contribution of sorbed tetrahedral Zn and Zn-Al-LDH in U, and from hemimorphite and Zn-Al-LDH in N (Fig. S3).

In the samples from the CW, Zn chemical speciation of the rhizospheres did not change significantly in comparison to the initial substrates (Fig. 5, Table S7, Fig. S4-S6). In all roots, a fraction of Zn contribution (14-22%) appeared to originate from residues of the rhizospheres (layered minerals, hemimorphite and smithsonite), supporting the qualitative XANES analysis (Fig. 5). In UCW-roots and NCW-roots, a high fraction (49-69%) of Zn was present in a disordered environment, like sorbed tetrahedral Zn, and in UCW-roots and SMCW-roots, we detected Zn bound to phosphate (18-23%) and to citrate (18-26%). A small portion (15%) of Zn was found in a Zn cysteine-like phase in NCW-roots. All the stems showed a similar Zn speciation, mainly sorbed Zn (up to 65%) and Zn cysteine (up to 35%). Zinc phosphate-like phase (13-20%) was detected in NCW-stems and SMCW-stems, although it is worth noting that UCW-stems were characterized by low Zn contents (41 mg/kg), resulting in high noise XANES spectra, and LCA could be affected by a quite large uncertainty.

For the ZnW samples, differences in the Zn chemical speciation were found, and they were different in the three systems, as observed for the Zn accumulation (Fig. 3 and Table S3) and distribution (Fig. 4 and Table S4). In UZnW-rhizo, we observed an increase in Zn-Al-LDH (from 25 to 48%), a decrease in the sorbed Zn (from 64% to 38%), and a contribution resembling Zn bound to cysteine (14%), compound not found in UCW-rhizo. Differently from samples belonging to the CW, Zn cysteine (18%) was observed in UZnW-roots, and Zn phosphate (16%) in UZnW-stems. In the Sa Masa rhizosphere and roots, Zn citrate increased from 19% (SMCW-rhizo) to 39% (SMZnW-rhizo), and from 26% SMCW-roots) to 48% (SMZnW-roots), respectively. In stems, the sorbed Zn decreased from 61% (SMCW-stems) to 16% (SMZnW-stems), Zn cysteine increased from 26% (SMCW-stems) to 42% (SMZnW-stems), and a portion of Zn (21%) was bound to citrate in SMZnW-stems. For the Naracauli samples (rhizosphere, roots and stems), we did not find significant differences in the Zn chemical speciation in the samples from the two irrigation lines.

Discussion

Rhizosphere-plant interactions and Zn pathway

Zinc plant uptake is affected by several factors such as Zn content at the soil-root interface, plant demand, and root absorption capacity (Sadeghzadeh, 2013). It remains a controversial issue whether plants predominantly absorb metal ions from soil solution (Kim et al., 2010) or from solid phases. Indeed, although the dissolved concentration in soil pore water is often used to estimate metal bioavailability, metals in minerals are key components, as plants can uptake elements from the non-mobile fractions of the solids and because the solid-phase pool controls the resupply of metals to the soil solution (Hinsinger and Courchesne, 2007; Knight et al., 1997; Zhang et al., 2001). Also, metal can be taken up by plants in form of nanoparticles, through various pathways driven by the specific materials, particle morphology and size, and by the plant species, growth stage, physiological and growing conditions (Adele et al., 2018; Lv et al., 2019; Tripathi et al., 2017). The sources of Zn in the investigated systems depended on the substrate origin and the irrigation line. In the mine-waste-rich substrates, Zn primary minerals, such as hemimorphite and smithsonite, were the most abundant Zn species as revealed by XRD (Table 2) and XANES (Fig. 6 and Table S7) analyses, and Zn ranged between ~10000 and ~20000 mg/kg. In the unpolluted substrate, Zn was mainly present as sorbed species and incorporated in layered minerals (XANES

data, Fig. 6 and Table S7), with a concentration of ~140 mg/kg. The detected species must be considered as dynamic Zn sources, as they are part of both biotic and abiotic bidirectional processes: from the roots to soil and from soil to the roots. Specifically, plant roots and microbial metabolism can transform metal species to facilitate metal uptake or to detoxify metals through root exudation, microorganism secretions and/or pH changes, leading to variable concentration gradients and speciation patterns, whose extent can vary through time (Adele et al., 2021; Brown et al., 1999; Kangwankraiphaisan et al., 2013; Kuzyakov and Razavi, 2019; Schnepf et al., 2022).

After five months of plant-mineral-water interaction, XRD analysis did not show any bulk mineralogical variation between the initial substrates and the rhizospheres for both the CW and the ZnW (Table 2), but dissolution-precipitation reactions were active as demonstrated by the formation of efflorescent salts on the substrate surface. Gypsum and hexahydrite occurred as byproduct of sulfide mineral oxidation (Jambor et al., 2000; Manoukian, 2016). In our substrate samples, XRD analysis did not show sulfide phases but, probably, they were present below the detection limit of 1% by volume. XANES analysis revealed that, in the efflorescent salts, Zn was present in three main phases: tetrahedral Zn, adsorbed or as hemimorphite, and octahedral Zn as in layered minerals. In natural environments, efflorescent salts act only as a temporary sink of Zn because their stability is affected by their solubility and the hydrological regime. When exposed to rain or to flowing surface waters, they can be dissolved quickly, contributing to the solute load of surface and pore water (Nordstrom, 1999), playing an important role in controlling water composition. We argue that the apparent lack of variation in the bulk mineralogical composition (crystallographic phases) between rhizosphere samples from the two irrigation lines is attributable to slow reaction kinetics and short experimental duration time. However, XANES analysis, which is more sensitive, revealed that Zn supplement to the irrigation water differently influenced the Zn chemical speciation in the investigated systems. For instance, high Zn contents in water led to an increase of Zn hosted in layered minerals in the unpolluted rhizosphere, from 25% (UCW-rhizo) to 48% (UZnW-rhizo). Previous studies (Voegelin et al. 2005, and references therein) have demonstrated that the incorporation of Zn in newly forming layered minerals (e.g. LDH, phyllosilicates, or hydroxide type) may represent an important metal sequestration mechanism in soils and sediments. This seems to be an active pathway also in this study. Moreover, Zn cysteine was detected in UZnW-rhizo and UZnW-roots; this species was not observed in the samples from the CW. In the Sa Masa system, Zn citrate increased both in the rhizosphere, from 19% (SMCW-rhizo) to 39% (SMZnW-rhizo), and in the roots, from 26% (SMCW-roots) to 48% (SMZnW-roots). In stems, adsorbed Zn decreased, from 61% (SMCW-stems) to 16% (SMZnW-stems), whereas Zn cysteine increased, from 26% (SMCW-stems) to 42% (SMZnW-stems), and Zn citrate was detected (species not found in SMCW-stems). Zinc cysteine formation (or increase) was probably due to *J. acutus* response to high Zn content in water, supporting previous findings on the relevant role of cysteine in metal homeostasis, detoxification and tolerance to high concentrations of Zn in many plants, because it helps to regulate (Domínguez-Solís et al., 2004; Oven et al., 2002) and reduce the cellular bioavailability of Zn (Adediran et al., 2016; Adele et al., 2021, 2018). XANES data suggested that also citrate plays a key role in the control of Zn bioavailability, as demonstrated by its increase in the Sa Masa samples from the ZnW. Indeed, citrate is a ligand involved in metal transport and storage in plants (Gramlich et al., 2013). For example, Terzano et al. (2008) found that, in the edible plant *Eruca vesicaria*, Zn accumulated outside the root endodermis with some Zn translocated in the xylem as Zn citrate. In shoots of the hyperaccumulator *Thlaspi caerulescens*, Zn citrate was the dominant species with hydrated Zn, histidine, cell wall, and oxalate playing a secondary role (Salt et al., 1999). In our experiment, the Zn supply by the water could have stimulated a higher citrate synthesis (Shen et al., 1997). Observed variations in Zn speciation for the epigean organs collected from the unpolluted and Sa Masa systems (CW vs ZnW) support results reported by Da Cruz et al. (2019) that performed time resolved experiments to investigate Zn uptake, biotransformation and physiological effects on *Phaseolus vulgaris* (L.) exposed to ZnO nanoparticles (40 and

300 nm) dispersions and $ZnSO_{4(aq)}$ (Zn 100 and 1000 mg/l) for 48 h. They observed that, in leaves, Zn is mainly present as Zn phosphate (59–87%) in all treatments, whereas Zn-histidine was detected for $ZnSO_4$, 40 and 300 nm ZnO exposures, and Zn-malate for the 300 nm treated plants, demonstrating that Zn speciation can change when the same plant species is exposed to different Zn sources.

Differently from the unpolluted and Sa Masa systems, the Naracauli system did not show any significant variation in the Zn coordination environment for the two irrigation lines. The occurrence of Zn phosphate in stems from the three systems is consistent with other studies. For instance, Zn phosphate was detected in the leaves of *Phaseolus vulgaris* (the common bean) from plants exposed to 10 mg/l Zn of $ZnSO_{4(aq)}$, and ZnO nanoparticles (40 nm and 300 nm) for seven days (da Cruz et al., 2019), and in the apoplasm of tobacco roots (Straczek et al., 2008).

Our results highlight the complexity of the interactions between the rhizosphere, water and plants, and demonstrate that metal transformation is affected by the Zn chemical species present in the rhizosphere minerals, and that *J. acutus* develops different complexations mechanisms when it is watered with Zn-spiked water. Such complexity is consistent with data reported by Wang et al. (2013) that examined the uptake and transformation of Zn in various tissues of cowpea (*Vigna unguiculata* (L.) Walp.) exposed to ZnO-NPs or soluble Zn ($ZnCl_2$) conducting both solution and soil (Oxisol, U.S. Soil Taxonomy) culture experiments. In solution culture, soluble Zn was more toxic than the ZnO-NPs, and a substantial accumulation of ZnO-NPs occurred on the root surface of plants exposed to ZnO-NPs. Specifically, XANES analysis showed that about 65% of the Zn in roots was present as ZnO-NPs, and 32% associated with histidine. In contrast, in roots exposed to $ZnCl_2$, Zn was associated with histidine (49%), polygalacturonic acid (ZnPGA, 32%), and Zn-phosphate (19%). In soil culture experiments, there was no significant difference in plant growth and accumulation or speciation of Zn between soluble Zn and ZnO-NP treatments, indicating that the added ZnO-NPs underwent rapid dissolution following their entry into the soil. The Zn in roots from both treatments was found to be associated with citrate (average 51%), histidine (28%), and phytate (20%). In stem tissues, for both soluble Zn and ZnO-NPs treatments (solution and soil culture), Zn citrate, Zn histidine and Zn phytate were detected, and their contributions were affected by the growth matrix, whereas the Zn treatment (ZnO-NPs or soluble Zn) did not affect significantly the concentration of the above-mentioned Zn species for the same growth matrix. It is worth noting that experiments developed by Wang et al. (2013) are not exactly comparable with ours as they added Zn, as either ZnO-NPs or $ZnCl_2$, in nutrient solutions (final Zn concentration 25 mg/l) or Oxisol (final Zn concentration 25 mg/kg), whereas we used an unpolluted substrate, two already contaminated growth substrates and two different Zn concentration in water. Nevertheless, both the researches contribute to achieve new fundamental knowledge for the understanding of Zn uptake and transformation in plants exposed to different Zn sources.

Plant growth and Zn accumulation

Zinc is one of the eight trace elements (along with Mn, Cu, B, Fe, Cl, Mo and Ni) that are essential for healthy growth and reproduction of plants (Vatansever et al., 2017). It is required as a structural component of many proteins, and an insufficient amount leads to physiological stresses due to the failure of Zn dependent metabolic processes (Sadeghzadeh, 2013), but excessive Zn (100-500 mg/kg in the vegetal tissues) is toxic to plants, and leads to functional and structural disorders (Balafrej et al., 2020; Kabata-Pendias, 2000; Zeng et al., 2011). In our experiment, plant growth (Fig. 2 and Table S2) was higher for specimens grown on the unpolluted substrate (CW 29±5 cm, ZnW 26±1 cm), followed by the Sa Masa (CW 17.3±0.9 cm, ZnW 15±1 cm) and the Naracauli (CW 12±1 cm, ZnW 11.8±0.7 cm) substrates. This behavior could be related to the high concentration of Zn (Balafrej et al., 2020) and other metals, such as Pb (~5220-20500 mg/kg) and Cd (~50-126 mg/kg), in the mine-waste-rich substrates (Bacchetta et al., 2015; Caboi et al., 1993; Loi, 1992), as *J.*

acutus can tolerate exogenous Zn concentrations up to 60-100 mM (Mateos-Naranjo et al., 2014; Santos et al., 2014). Indeed, in roots and stems from the unpolluted substrate (CW and ZnW), Zn was lower than 100-500 mg/kg, thus probably not affecting the metabolic processes (Kabata-Pendias, 2000; Zeng et al., 2011), whereas in roots and stems from the polluted substrates Zn ranged between 4400-10000 mg/kg and 420-1140 mg/kg, respectively. Our findings support results from Mateos-Naranjo et al. (2014) who performed a pot experiment (with perlite as growth substrate and 20% Hoagland's solution + $ZnSO_4 \cdot 7H_2O$, Zn from 0 to 100 mM). They observed increasing Zn contents in *J. acutus* tissues (up to 2500 mg/kg in roots, and up to 500 mg/kg in stems) when the plants were irrigated with solutions characterized by high Zn concentrations. In their experiment, the mean plant height was smaller in 100 mM Zn treatment than in control (Zn 0 mM). In our experiment, plant development appeared to be affected more by the composition of the substrate than by the Zn content in the water, that did not significantly affect the plant height for a specific growth substrate (Fig. 2 and Table S2).

Despite the negligible influence of the Zn content in water on plant growth, comparing samples belonging to the CW and the ZnW, some differences were observed in the Zn accumulation (Fig. 3 and Table S3) and distribution (Fig. 4 and Table S4), and they varied for the three investigated systems. The greatest variations were observed for the samples collected from the unpolluted group. Specifically, despite the increase in the Zn concentration in UZnW-rhizo, -roots and -stems, the BCF, BAC and TF decreased, suggesting that a lower Zn accumulation and translocation occurred when the Zn concentration in the water was higher. This trend could be due to the incorporation of Zn in low bioavailable forms in the rhizosphere (i.e., Zn-Al-LDH in UZnW sample) and/or to complexation mechanisms induced by *J. acutus* to control Zn uptake (i.e., Zn cysteine). On the contrary, the experiments carried out in the already polluted substrates pointed out a minority role of the Zn content in the water that had no significant effects on the Zn accumulation in stems (BAC values) and on its translocation (TF values) (Fig. 4 and Table S4).

Conclusions

Understanding the interactions between metals and plants is a fundamental issue we must face because metals released into the environment will inevitably interact with plants, which are basic components of ecosystems. Moreover, revealing metal mobilization/immobilization processes at the molecular level is fundamental to develop efficient remediation strategies based on phytoremediation. Our results provide a thorough multi-technique characterization of the rhizosphere-plant system of *J. acutus* exposed to different Zn sources. Zinc excess in the growth substrate negatively affected the plant growth, whereas, for a specific substrate, the Zn content in the irrigation water did not significantly influence the plant height. Therefore, in the investigated systems, soil properties apparently had a more important role on the plant health status than water composition. Within the rhizosphere and the vegetal tissues, Zn chemical speciation depended on the mineralogical composition of the initial substrate and on different complexation mechanisms developed by *J. acutus* when exposed to different Zn sources. From the rhizosphere to the roots, we observed an increase in the amount of Zn associated with citrate, cysteine, phosphate, or adsorbed Zn. XRD patterns did not reveal the presence of crystalline Zn phases in *J. acutus* roots, as in *J. acutus* plants spontaneously growing in mining areas, but XANES analysis identified Zn in layered minerals (unpolluted, Naracauli and Sa Masa), hemimorphite and smithsonite (Sa Masa). Although a biological origin for these phases cannot be fully excluded, their occurrence could be due to a strong adhesion of the rhizosphere minerals to the epidermis, induced by the production of root exudates. Moreover, we cannot exclude Zn uptake by *J. acutus* as amorphous solid phase(s), as different plant species are able to uptake and translocate metals as nanoparticles. A lower Zn translocation (lower TF values) occurred in plants grown on the contaminated substrates that, we argue, allows to

prevent excessive Zn accumulation in the epigean organs, avoiding detrimental effects to the plant health. Irrigation with the Zn-spiked water led to variable increases in the total Zn concentration in the vegetal tissues, and Zn distribution varied for the investigated systems. We hypothesize that Zn accumulation and detoxification was driven by changes in its speciation, namely variation in the amount of Zn citrate and Zn cysteine. The watering with Zn-spiked water did not lead to similar variations in the distribution of the different Zn complexes for the investigated rhizosphere-plant systems, suggesting that Zn transformation was mainly driven by rhizosphere minerals.

With this study, we demonstrated that *J. acutus* is not only capable of developing site-specific tolerance mechanisms, but it is also capable of differently modulating Zn transformation when Zn is additionally supplied by watering. Further studies are required to improve our understanding and to reveal the spatial-temporal gradients driven by specific geo-bio interactions among the selected plant species, the rhizosphere microorganisms, minerals and water.

Acknowledgments

The authors acknowledge: the CERIC-ERIC Consortium (grant number: 20167045) for the access to the XAFS beamline and financial support; the MCX beamline (experiment number #20140061); the XRF beamline; CESA (E58C16000080003) from RAS, FdS (F72F16003080002, and "Sustainable land management: the tools of geology for the environment" - F75F21001270007) grants; CM acknowledges the grant Dipartimento di Eccellenza, MIUR (ARTICOLO 1, COMMI 314 e 337 LEGGE 232/2016).

References

Adediran, G.A., Ngwenya, B.T., Mosselmans, J.F.W., Heal, K. V, 2016. Bacteria-zinc co-localization implicates enhanced synthesis of cysteine-rich peptides in zinc detoxification when *Brassica juncea* is inoculated with *Rhizobium leguminosarum*. New Phytol. 209, 280–293. https://doi.org/10.1111/nph.13588

Adediran, G.A., Ngwenya, B.T., Mosselmans, J.F.W., Heal, K. V, Harvie, B.A., 2015. Mechanisms behind bacteria induced plant growth promotion and Zn accumulation in *Brassica juncea*. J. Hazard. Mater. 283, 490–499. https://doi.org/10.1016/j.jhazmat.2014.09.064

Adele, N.C., Ngwenya, B.T., Heal, K. V, Mosselmans, J.F.W., 2021. Role of plant growth promoting bacteria in driving speciation gradients across soil-rhizosphere-plant interfaces in zinc-contaminated soils. Environ. Pollut. 279, 116909. https://doi.org/https://doi.org/10.1016/j.envpol.2021.116909

Adele, N.C., Ngwenya, B.T., Heal, K. V, Mosselmans, J.F.W., 2018. Soil Bacteria Override Speciation Effects on Zinc Phytotoxicity in Zinc-Contaminated Soils. Environ. Sci. Technol. 52, 3412–3421. https://doi.org/10.1021/acs.est.7b05094

Alam, M.R., Rahman, M.M., Tam, N.F.-Y., Yu, R.M.K., MacFarlane, G.R., 2022. The accumulation and distribution of arsenic species and selected metals in the saltmarsh halophyte, spiny rush (*Juncus acutus*). Mar. Pollut. Bull. 175, 113373. https://doi.org/https://doi.org/10.1016/j.marpolbul.2022.113373

Aydın Temel, F., Avcı, E., Ardalı, Y., 2018. Full scale horizontal subsurface flow constructed wetlands to treat domestic wastewater by *Juncus acutus* and *Cortaderia selloana*. Int. J. Phytoremediation 20, 264–273. https://doi.org/10.1080/15226514.2017.1374336

519 Bacchetta, G., Cappai, G., Carucci, A., Tamburini, E., 2015. Use of native plants for the remediation of
520 abandoned mine sites in mediterranean semiarid environments. Bull. Environ. Contam. Toxicol. 94, 326–
521 333. https://doi.org/10.1007/s00128-015-1467-y
522 Balafrej, H., Bogusz, D., Abidine Triqui, Z.-E., Guedira, A., Bendaou, N., Smouni, A., Fahr, M., 2020. Zinc
523 hyperaccumulation in plants: A review. Plants 9, 562. https://doi.org/10.3390/plants9050562
524 Bao, Z., Al, T., Bain, J., Shrimpton, H.K., Finfrock, Y.Z., Ptacek, C.J., Blowes, D.W., 2022. Sphalerite
525 weathering and controls on Zn and Cd migration in mine waste rock: An integrated study from the
526 molecular scale to the field scale. Geochim. Cosmochim. Acta 318, 1–18.
527 https://doi.org/https://doi.org/10.1016/j.gca.2021.11.007
528 Boi, M.E., Medas, D., Aquilanti, G., Bacchetta, G., Birarda, G., Cappai, G., Carlomagno, I., Casu, M.A.,
529 Gianoncelli, A., Meneghini, C., Piredda, M., Podda, F., Porceddu, M., Rimondi, V., Vaccari, L., De
530 Giudici, G., 2020. Mineralogy and Zn Chemical Speciation in a Soil-Plant System from a Metal-Extreme
531 Environment: A Study on Helichrysum microphyllum subsp. tyrrhenicum (Campo Pisano Mine, SW
532 Sardinia, Italy). Minerals 10, 259. https://doi.org/10.3390/min10030259
533 Boni, M., Gilg, H.A., Aversa, G., Balassone, G., 2003. The "Calamine" of Southwest Sardinia: geology,
534 mineralogy, and stable isotope geochemistry of supergene Zn mineralization. Econ. Geol. 98, 731–748.
535 https://doi.org/10.2113/gsecongeo.98.4.731
536 Briffa, J., Sinagra, E., Blundell, R., 2020. Heavy metal pollution in the environment and their toxicological
537 effects on humans. Heliyon 6, e04691. https://doi.org/10.1016/j.heliyon.2020.e04691
538 Brooks, R., 2008. Plants that hyperaccumulate heavy metals, in: Plants and the Chemical Elements:
539 Biochemistry, Uptake, Tolerance and Toxicity. pp. 87–105. https://doi.org/10.1002/9783527615919.ch4
540 Brown, G.E., Foster, A.L., Ostergren, J.D., 1999. Mineral surfaces and bioavailability of heavy metals: A
541 molecular-scale perspective. Proc. Natl. Acad. Sci. 96, 3388 LP – 3395.
542 https://doi.org/10.1073/pnas.96.7.3388
543 Brown, K., Bettink, K., 2006. Biology of sharp rush *Juncus acutus*. Manangin sharp rush Juncus acutus. Proc.
544 a Work. held Wollast. Coll. Conf. Cent. 38–42.
545 Caboi, R., Cidu, R., Cristini, A., Fanfani, L., Massoli-Novelli, R., Zuddas, P., 1993. The abandoned Pb-Zn
546 mine of Ingurtosu, Sardinia (Italy). Eng. Geol. 34, 211–218. https://doi.org/10.1016/0013-
547 7952(93)90090-Y
548 Caldelas, C., Weiss, D.J., 2017. Zinc homeostasis and isotopic fractionation in plants: a review. Plant Soil 411,
549 17–46. https://doi.org/10.1007/s11104-016-3146-0
550 Chandrakasan, G., Toledano Ayala, M., García Trejo, J.F., Marcus, G., Carroll, D.L., 2021. Mapping and
551 distribution of speciation changes of metals from nanoparticles in environmental matrices using
552 synchrotron radiation techniques. Environ. Nanotechnology, Monit. Manag. 16, 100491.
553 https://doi.org/https://doi.org/10.1016/j.enmm.2021.100491
554 Chen, K.Y., Yang, P.T., Chang, H.F., Yeh, K.C., Wang, S.L., 2022. Soil gallium speciation and resulting
555 gallium uptake by rice plants. J. Hazard. Mater. 424, 127582.

https://doi.org/https://doi.org/10.1016/j.jhazmat.2021.127582
Christofilopoulos, S., Syranidou, E., Gkavrou, G., Manousaki, E., Kalogerakis, N., 2016. The role of halophyte *Juncus acutus* L. in the remediation of mixed contamination in a hydroponic greenhouse experiment. J. Chem. Technol. Biotechnol. 91, 1665–1674. https://doi.org/10.1002/jctb.4939
Cidu, R., Biddau, R., 2005. Legacy at abandoned mines: impact of mine wastes on surface waters, in: Proceeding of the 9th International Mine Water Association Congress (IMWA). pp. 247–252.
Cidu, R., Frau, F., Da Pelo, S., 2011. Drainage at Abandoned Mine Sites: Natural Attenuation of Contaminants in Different Seasons. Mine Water Environ. 30, 113–126. https://doi.org/10.1007/s10230-011-0146-4
da Cruz, T.N.M., Savassa, S.M., Montanha, G.S., Ishida, J.K., de Almeida, E., Tsai, S.M., Lavres Junior, J., Pereira de Carvalho, H.W., 2019. A new glance on root-to-shoot in vivo zinc transport and time-dependent physiological effects of $ZnSO_4$ and ZnO nanoparticles on plants. Sci. Rep. 9, 10416. https://doi.org/10.1038/s41598-019-46796-3
De Giudici, G., Lattanzi, P., Medas, D., 2015. Synchrotron radiation and environmental sciences, in: Mobilio S., Boscherini F., M.C. (Ed.), Synchrotron Radiation: Basics, Methods and Applications. Springer Berlin Heidelberg, pp. 661–676. https://doi.org/10.1007/978-3-642-55315-8_25
De Giudici, G., Pusceddu, C., Medas, D., Meneghini, C., Gianoncelli, A., Rimondi, V., Podda, F., Cidu, R., Lattanzi, P., Wanty, R.B., Kimball, B.A., 2017. The role of natural biogeochemical barriers in limiting metal loading to a stream affected by mine drainage. Appl. Geochemistry 76, 124–135. https://doi.org/10.1016/j.apgeochem.2016.11.020
de la Fuente, V., Rufo, L., Sánchez-Gavilán, I., Ramírez, E., Rodríguez, N., Amils, R., 2018. Plant Tissues and Embryos Biominerals in *Sarcocornia pruinosa*, a Halophyte from the Río Tinto Salt Marshes. Minerals. https://doi.org/10.3390/min8110505
Di Cicco, A., Aquilanti, G., Minicucci, M., Principi, E., Novello, N., Cognigni, A., Olivi, L., 2009. Novel XAFS capabilities at ELETTRA synchrotron light source. J. Phys. Conf. Ser. 190, 12043. https://doi.org/10.1088/1742-6596/190/1/012043
Domínguez-Solís, J.R., López-Martín, M.C., Ager, F.J., Ynsa, M.D., Romero, L.C., Gotor, C., 2004. Increased cysteine availability is essential for cadmium tolerance and accumulation in Arabidopsis thaliana. Plant Biotechnol. J. 2, 469–476. https://doi.org/10.1111/j.1467-7652.2004.00092.x
Doolette, C.L., Read, T.L., Li, C., Scheckel, K.G., Donner, E., Kopittke, P.M., Schjoerring, J.K., Lombi, E., 2018. Foliar application of zinc sulphate and zinc EDTA to wheat leaves: differences in mobility, distribution, and speciation. J. Exp. Bot. 69, 4469–4481. https://doi.org/10.1093/jxb/ery236
Dore, E., Fancello, D., Rigonat, N., Medas, D., Cidu, R., Da Pelo, S., Frau, F., Lattanzi, P., Marras, P.A., Meneghini, C., Podda, F., Rimondi, V., Runkel, R.L., Kimball, B., Wanty, R.B., De Giudici, G., 2020. Natural attenuation can lead to environmental resilience in mine environment. Appl. Geochemistry 117. https://doi.org/10.1016/j.apgeochem.2020.104597
Duarte, B., Durante, L., Marques, J.C., Reis-Santos, P., Fonseca, V.F., Caçador, I., 2021. Development of a toxicophenomic index for trace element ecotoxicity tests using the halophyte Juncus acutus: Juncus-

TOX. Ecol. Indic. 121, 107097. https://doi.org/10.1016/j.ecolind.2020.107097
Etschmann, B.E., Donner, E., Brugger, J., Howard, D.L., de Jonge, M.D., Paterson, D., Naidu, R., Scheckel, K.G., Ryan, C.G., Lombi, E., 2014. Speciation mapping of environmental samples using XANES imaging. Environ. Chem. 11, 341–350. https://doi.org/10.1071/EN13189
Fancello, D., Scalco, J., Medas, D., Rodeghero, E., Martucci, A., Meneghini, C., De Giudici, G., 2019. XRD-thermal combined analyses: An approach to evaluate the potential of phytoremediation, phytomining, and biochar production. Int. J. Environ. Res. Public Health 16. https://doi.org/10.3390/ijerph16111976
Fellet, G., Marchiol, L., Perosa, D., Zerbi, G., 2007. The application of phytoremediation technology in a soil contaminated by pyrite cinders. Ecol. Eng. 31, 207–214. https://doi.org/10.1016/j.ecoleng.2007.06.011
Fourati, E., Vogel-Mikuš, K., Wali, M., Kavčič, A., Gomilšek, J.P., Kodre, A., Kelemen, M., Vavpetič, P., Pelicon, P., Abdelly, C., Ghnaya, T., 2020. Nickel tolerance and toxicity mechanisms in the halophyte *Sesuvium portulacastrum* L. as revealed by Ni localization and ligand environment studies. Environ. Sci. Pollut. Res. 27, 23402–23410. https://doi.org/10.1007/s11356-019-05209-8
Freitas, M., Pacheco, A.M.G., Anawar, H., Canha, N., Dionisio, I., Bettencourt, A., Henriques, F., Gomes, C., Capelo, S., 2009. Determination of phytoextraction potential of plant species for toxic elements in soils of abandoned sulphide-mining areas. J. Radioanal. Nucl. Chem. 282, 21–27. https://doi.org/10.1007/s10967-009-0222-4
Frérot, H., Lefèbvre, C., Gruber, W., Collin, C., Santos, A. Dos, Escarré, J., 2006. Specific Interactions between Local Metallicolous Plants Improve the Phytostabilization of Mine Soils. Plant Soil 282, 53–65. https://doi.org/10.1007/s11104-005-5315-4
Gaur, A., Shrivastava, B., 2012. A Comparative Study of the Methods of Speciation Using X-ray Absorption Fine Structure. Acta Phys. Pol. Ser. a 121, 647–652. https://doi.org/10.12693/APhysPolA.121.647
Gramlich, A., Tandy, S., Frossard, E., Eikenberg, J., Schulin, R., 2013. Availability of Zinc and the Ligands Citrate and Histidine to Wheat: Does Uptake of Entire Complexes Play a Role? J. Agric. Food Chem. 61, 10409–10417. https://doi.org/10.1021/jf401117d
Hammersley, A.P., Svensson, S.O., Hanfland, M., Fitch, A.N., Hausermann, D., 1996. Two-dimensional detector software: From real detector to idealised image or two-theta scan. High Press. Res. 14, 235–248. https://doi.org/10.1080/08957959608201408
Hinsinger, P., Courchesne, F., 2007. Biogeochemistry of Metals and Metalloids at the Soil–Root Interface, in: Violante, A., Huang, P.M., Gadd, G.M. (Eds.), Biophysico-Chemical Processes of Heavy Metals and Metalloids in Soil Environments. pp. 265–311. https://doi.org/10.1002/9780470175484.ch7
Hylander, L.D., 2002. Improvements of rhizoboxes used for studies of soil–root interactions. Commun. Soil Sci. Plant Anal. 33, 155–161. https://doi.org/10.1081/CSS-120002384
Jambor, J.L., Nordstrom, D.K., Alpers, C.N., 2000. Metal-sulfate Salts from Sulfide Mineral Oxidation. Rev. Mineral. Geochemistry 40, 303–350. https://doi.org/10.2138/rmg.2000.40.6
Jark, W., Eichert, D., Lühl, L., Gambitta, A., 2014. Optimisation of a compact optical system for the beamtransport at the X-ray Fluorescence beamline at Elettra for experiments with small spots. Proc SPIE

9207, 92070G. https://doi.org/10.1117/12.2063009
Kabata-Pendias, A., 2000. Trace Elements in Soils and Plants. CRC Press, Boca Raton, FL, Boca Raton.
Kangwankraiphaisan, T., Suntornvongsagul, K., Sihanonth, P., Klysubun, W., Gadd, G., 2013. Influence of arbuscular mycorrhizal fungi (AMF) on zinc biogeochemistry in the rhizosphere of *Lindenbergia philippensis* growing in zinc-contaminated sediment. Biometals 26, 489–505. https://doi.org/10.1007/s10534-013-9634-2
Karydas, A.G., Czyzycki, M., Leani, J.J., Migliori, A., Osan, J., Bogovac, M., Wrobel, P., Vakula, N., Padilla-Alvarez, R., Menk, R.H., Gol, M.G., Antonelli, M., Tiwari, M.K., Caliri, C., Vogel-Mikuš, K., Darby, I., Kaiser, R.B., 2018. An IAEA multi-technique X-ray spectrometry endstation at Elettra Sincrotrone Trieste: benchmarking results and interdisciplinary applications. J. Synchrotron Radiat. 25, 189–203. https://doi.org/10.1107/S1600577517016332
Kim, K.R., Owens, G., Naidu, R., 2010. Effect of Root-Induced Chemical Changes on Dynamics and Plant Uptake of Heavy Metals in Rhizosphere Soils. Pedosphere 20, 494–504. https://doi.org/10.1016/S1002-0160(10)60039-2
Knight, B., Zhao, F.J., McGrath, S.P., Shen, Z.G., 1997. Zinc and cadmium uptake by the hyperaccumulator Thlaspi caerulescens in contaminated soils and its effects on the concentration and chemical speciation of metals in soil solution. Plant Soil 197, 71–78. https://doi.org/10.1023/A:1004255323909
Kopittke, P.M., Wang, P., Lombi, E., Donner, E., 2017. Synchrotron-based X-Ray Approaches for Examining Toxic Trace Metal(loid)s in Soil–Plant Systems. J. Environ. Qual. 46, 1175–1189. https://doi.org/10.2134/jeq2016.09.0361
Kothe, E., Büchel, G., 2014. UMBRELLA: Using MicroBes for the REgulation of heavy metaL mobiLity at ecosystem and landscape scAle. Environ. Sci. Pollut. Res. 21, 6761–6764. https://doi.org/10.1007/s11356-014-2689-y
Kuzyakov, Y., Razavi, B.S., 2019. Rhizosphere size and shape: Temporal dynamics and spatial stationarity. Soil Biol. Biochem. 135, 343–360. https://doi.org/10.1016/j.soilbio.2019.05.011
Kwon, M.J., Boyanov, M.I., Mishra, B., Kemner, K.M., Jeon, S., Hong, J.K., Lee, S., 2022. Zn speciation and Fate in Soils and Sediments Along the Ground Transportation Route of Zn Ore to a Smelter. J. Hazard. Mater. 129422. https://doi.org/https://doi.org/10.1016/j.jhazmat.2022.129422
Landsberger, S., Robinson, S., Freitas, M., Canha, N., Pacheco, A., Anawar, H., 2010. Characterisation of antimony, arsenic, cadmium, copper and tin occurrences at an abandoned sulphide-mining area. Int. J. Environ. Heal. 4, 166–180. https://doi.org/10.1504/IJENVH.2010.033706
Loi, M., 1992. Studio degli sterili della miniera di Ingurtosu e loro interazione con le acque del Rio Naracauli. Degree thesis, University of Cagliari.
Lombardo, A., 1982. Flora Montevidensis. Intendencia Municipal de Montevideo. Flora Montevidensis. Intend. Munic. Montevideo 1, 366–367.
López-Juambeltz, F., Rodríguez-Gallego, L., Dabezíes, J.M., Chreties, C., Narbondo, S., Conde, D., 2020. A GIS-based assessment combined with local ecological knowledge to support the management of *Juncus*

667 *acutus* L. spreading in the floodplain of a protected coastal lagoon. J. Nat. Conserv. 57, 125891.
668 https://doi.org/https://doi.org/10.1016/j.jnc.2020.125891
669 Lv, J., Christie, P., Zhang, S., 2019. Uptake, translocation, and transformation of metal-based nanoparticles in
670 plants: recent advances and methodological challenges. Environ. Sci. Nano 6, 41–59.
671 https://doi.org/10.1039/C8EN00645H
672 Manceau, A., Marcus, M., Lenoir, T., 2014. Estimating the number of pure chemical components in a mixture
673 by X-ray absorption spectroscopy. J. Synchrotron Radiat. 21, 1140–1147.
674 https://doi.org/10.1107/S1600577514013526
675 Manoukian, L., 2016. Geochemical Characterization of Coexisting Precipitates and Waters from High-
676 Sulfidation Epithermal Gold Deposits. Queen's University.
677 Marchand, L., Mench, M., Jacob, D.L., Otte, M.L., 2010. Metal and metalloid removal in constructed wetlands,
678 with emphasis on the importance of plants and standardized measurements: A review. Environ. Pollut.
679 158, 3447–3461. https://doi.org/https://doi.org/10.1016/j.envpol.2010.08.018
680 Marchiol, L., Felle, t G., Boscutti, F., Montella, C., Mozzi, R., Guarino, C., 2013. Gentle remediation at the
681 former "Pertusola Sud" zinc smelter: evaluation of native species for phytoremediation purposes. Ecol.
682 Eng. 53, 343–353. https://doi.org/10.1016/j.ecoleng.2012.12.072
683 Mateos-Naranjo, E., Castellanos, E.M., Perez-Martin, A., 2014. Zinc tolerance and accumulation in the
684 halophytic species *Juncus acutus*. Environ. Exp. Bot. 100, 114–121.
685 https://doi.org/10.1016/j.envexpbot.2013.12.023
686 Mateos-Naranjo, E., Pérez-Romero, J.A., Redondo-Gómez, S., Mesa-Marín, J., Castellanos, E.M., Davy, A.J.,
687 2018. Salinity alleviates zinc toxicity in the saltmarsh zinc-accumulator *Juncus acutus*. Ecotoxicol.
688 Environ. Saf. 163, 478–485. https://doi.org/10.1016/j.ecoenv.2018.07.092
689 Medas, D., Carlomagno, I., Meneghini, C., Aquilanti, G., Araki, T., Bedolla, D.E., Buosi, C., Casu, M.A.,
690 Gianoncelli, A., Kuncser, A.C., Maraloiu, V.A., Giudici, G. De, 2018. Zinc incorporation in marine
691 bivalve shells grown in mine-polluted seabed sediments : a case study in the Malfidano mining area (SW
692 Sardinia , Italy). Environ. Sci. Pollut. Res. https://doi.org/10.1007/s11356-018-3504-y
693 Medas, D., Cidu, R., De Giudici, G., Podda, F., 2013. Geochemistry of rare earth elements in water and solid
694 materials at abandoned mines in SW Sardinia (Italy). J. Geochemical Explor. 133.
695 https://doi.org/10.1016/j.gexplo.2013.05.005
696 Medas, D., De Giudici, G., Pusceddu, C., Casu, M.A., Birarda, G., Vaccari, L., Gianoncelli, A., Meneghini,
697 C., 2019. Impact of Zn excess on biomineralization processes in *Juncus acutus* grown in mine polluted
698 sites. J. Hazard. Mater. 370, 98–107. https://doi.org/10.1016/j.jhazmat.2017.08.031
699 Montanha, G.S., Rodrigues, E.S., Romeu, S.L.Z., de Almeida, E., Reis, A.R., Lavres, J., Pereira de Carvalho,
700 H.W., 2020. Zinc uptake from $ZnSO_4$ (aq) and Zn-EDTA (aq) and its root-to-shoot transport in soybean
701 plants (*Glycine max*) probed by time-resolved *in vivo* X-ray spectroscopy. Plant Sci. 292, 110370.
702 https://doi.org/https://doi.org/10.1016/j.plantsci.2019.110370
703 Nordstrom, D.K., 1999. Efflorescent salts and their effect on water quality and mine plugging, in: IMWA

Proceedings 1999. p. 4.
Oven, M., Grill, E., Golan-Goldhirsh, A., Kutchan, T.M., Zenk, M.H., 2002. Increase of free cysteine and citric acid in plant cells exposed to cobalt ions. Phytochemistry 60, 467–474. https://doi.org/10.1016/S0031-9422(02)00135-8
Panfili, F., Manceau, A., Sarret, G., Spadini, L., Kirpichtchikova, T., Bert, V., Laboudigue, A., Marcus, M.A., Ahamdach, N., Libert, M.-F., 2005. The effect of phytostabilization on Zn speciation in a dredged contaminated sediment using scanning electron microscopy, X-ray fluorescence, EXAFS spectroscopy, and principal components analysis. Geochim. Cosmochim. Acta 69, 2265–2284. https://doi.org/https://doi.org/10.1016/j.gca.2004.10.017
Parsons, J.G., Aldrich, M. V, Gardea-Torresdey, J.L., 2002. Environmental and biological applications of extended X-ray absorption fine structure (EXAFS) and X-ray absorption near edge structure (XANES) spectroscopies. Appl. Spectrosc. Rev. 37, 187–222. https://doi.org/10.1081/ASR-120006044
Pavoni, E., Covelli, S., Adami, G., Baracchini, E., Cattelan, R., Crosera, M., Higueras, P., Lenaz, D., Petranich, E., 2018. Mobility and fate of Thallium and other potentially harmful elements in drainage waters from a decommissioned Zn-Pb mine (North-Eastern Italian Alps). J. Geochemical Explor. 188, 1–10. https://doi.org/https://doi.org/10.1016/j.gexplo.2018.01.005
Pérez-Esteban, J., Escolástico, C., Moliner, A., Masaguer, A., Ruiz-Fernández, J., 2014. Phytostabilization of metals in mine soils using *Brassica juncea* in combination with organic amendments. Plant Soil 377, 97–109. https://doi.org/10.1007/s11104-013-1629-9
Ravel, B., Newville, M., 2005. ATHENA, ARTEMIS, HEPHAESTUS: data analysis for X-ray absorption spectroscopy using IFEFFIT. J. Synchrotron Radiat. 12, 537–541. https://doi.org/10.1107/S0909049505012719
Rebuffi, L., Plaisier, J.R., Abdellatief, M., Lausi, A., Scardi, A.P., 2014. Mcx: A synchrotron radiation beamline for X-ray diffraction line profile analysis. Zeitschrift fur Anorg. und Allg. Chemie 640, 3100–3106. https://doi.org/10.1002/zaac.201400163
Sadeghzadeh, B., 2013. A review of zinc nutrition and plant breeding. J. soil Sci. plant Nutr. 13, 905–927. https://doi.org/10.4067/S0718-95162013005000072
Salt, D.E., Blaylock, M., Kumar, N.P.B.A., Dushenkov, V., Ensley, B.D., Chet, I., Raskin, I., 1995. Phytoremediation: a novel strategy for the removal of toxic metals from the environment using plants. Bio/Technology 13, 468–474. https://doi.org/10.1038/nbt0595-468
Salt, D.E., Prince, R.C., Baker, A.J.M., Raskin, I., Pickering, I.J., 1999. Zinc Ligands in the Metal Hyperaccumulator *Thlaspi caerulescens* As Determined Using X-ray Absorption Spectroscopy. Environ. Sci. Technol. 33, 713–717. https://doi.org/10.1021/es980825x
Santos, D., Duarte, B., Caçador, I., 2014. Unveiling Zn hyperaccumulation in *Juncus acutus*: Implications on the electronic energy fluxes and on oxidative stress with emphasis on non-functional Zn-chlorophylls. J. Photochem. Photobiol. B Biol. 140, 228–239. https://doi.org/10.1016/j.jphotobiol.2014.07.019
Saraswat, S., Rai, J.P.N., 2011. Complexation and detoxification of Zn and Cd in metal accumulating plants.

Rev. Environ. Sci. Bio/Technology 10, 327–339. https://doi.org/10.1007/s11157-011-9250-y

Sarret, G., Harada, E., Choi, Y.E., Isaure, M.P., Geoffroy, N., Fakra, S., Marcus, M.A., Birschwilks, M., Clemens, S., Manceau, A., 2006. Trichomes of tobacco excrete zinc as zinc-substituted calcium carbonate and other zinc-containing compounds. Plant Physiol. 141, 1021–1034. https://doi.org/10.1104/pp.106.082743

Sarret, G., Saumitou-Laprade, P., Bert, V., Proux, O., Hazemann, J.-L., Traverse, A., Marcus, M.A., Manceau, A., 2002. Forms of Zinc Accumulated in the Hyperaccumulator *Arabidopsis halleri*. Plant Physiol. 130, 1815 LP – 1826. https://doi.org/10.1104/pp.007799

Sarret, G., Smits, E.A.H.P., Michel, H.C., Isaure, M.P., Zhao, F.J., Tappero, R., 2013. Chapter One - Use of Synchrotron-Based Techniques to Elucidate Metal Uptake and Metabolism in Plants, in: Sparks, D.L.B.T.-A. in A. (Ed.), Advances in Agronomy. Academic Press, pp. 1–82. https://doi.org/10.1016/B978-0-12-407247-3.00001-9

Schnepf, A., Carminati, A., Ahmed, M.A., Ani, M., Benard, P., Bentz, J., Bonkowski, M., Knott, M., Diehl, D., Duddek, P., Kröner, E., Javaux, M., Landl, M., Lehndorff, E., Lippold, E., Lieu, A., Mueller, C.W., Oburger, E., Otten, W., Portell, X., Phalempin, M., Prechtel, A., Schulz, R., Vanderborght, J., Vetterlein, D., 2022. Linking rhizosphere processes across scales: Opinion. Plant Soil. https://doi.org/10.1007/s11104-022-05306-7

Shen, Z.G., Zhao, F.J., McGrath, S.P., 1997. Uptake and transport of zinc in the hyperaccumulator *Thlaspi caerulescens* and the non-hyperaccumulator *Thlaspi ochroleucum*. Plant. Cell Environ. 20, 898–906. https://doi.org/https://doi.org/10.1046/j.1365-3040.1997.d01-134.x

Shi, J., Wu, B., Yuan, X., YY, C., Chen, X., Chen, Y., Hu, T., 2008. An X-ray absorption spectroscopy investigation of speciation and biotransformation of copper in *Elsholtzia splendens*. Plant Soil 302, 163–174. https://doi.org/10.1007/s11104-007-9463-6

Sparks, E.L., Cebrian, J., Biber, P.D., Sheehan, K.L., Tobias, C.R., 2013. Cost-effectiveness of two small-scale salt marsh restoration designs. Ecol. Eng. 53, 250–256. https://doi.org/10.1016/j.ecoleng.2012.12.053

Sprocati, A.R., Alisi, C., Pinto, V., Montereali, M.R., Marconi, P., Tasso, F., Turnau, K., De Giudici, G., Goralska, K., Bevilacqua, M., Marini, F., Cremisini, C., 2014. Assessment of the applicability of a "toolbox" designed for microbially assisted phytoremediation: the case study at Ingurtosu mining site (Italy). Environ. Sci. Pollut. Res. 21, 6939–6951. https://doi.org/10.1007/s11356-013-2154-3

Stefani, A., Arduini, I., Onnis, A., 1991. *Juncus acutus*: germination and initial growth in presence of heavy metals. Ann. Bot. Fenn. 28, 37–43.

Straczek, A., Sarret, G., Manceau, A., Hinsinger, P., Geoffroy, N., Jaillard, B., 2008. Zinc distribution and speciation in roots of various genotypes of tobacco exposed to Zn. Environ. Exp. Bot. 63, 80–90. https://doi.org/https://doi.org/10.1016/j.envexpbot.2007.10.034

Syranidou, E., Christofilopoulos, S., Gkavrou, G., Thijs, S., Weyens, N., Vangronsveld, J., Kalogerakis, N., 2016. Exploitation of Endophytic Bacteria to Enhance the Phytoremediation Potential of the Wetland

Helophyte *Juncus acutus*. Front. Microbiol. 7, 1016. https://doi.org/10.3389/fmicb.2016.01016

Syranidou, E., Christofilopoulos, S., Kalogerakis, N., 2017a. *Juncus* spp.—The helophyte for all (phyto)remediation purposes? N. Biotechnol. 38, 43–55. https://doi.org/10.1016/j.nbt.2016.12.005

Syranidou, E., Christofilopoulos, S., Politi, M., Weyens, N., Venieri, D., Vangronsveld, J., Kalogerakis, N., 2017b. Bisphenol-A removal by the halophyte *Juncus acutus* in a phytoremediation pilot: Characterization and potential role of the endophytic community. J. Hazard. Mater. 323, 350–358. https://doi.org/10.1016/j.jhazmat.2016.05.034

Terzano, R., Al Chami, Z., Vekemans, B., Janssens, K., Miano, T., Ruggiero, P., 2008. Zinc Distribution and Speciation within Rocket Plants (*Eruca vesicaria* L. *Cavalieri*) Grown on a Polluted Soil Amended with Compost as Determined by XRF Microtomography and Micro-XANES. J. Agric. Food Chem. 56, 3222–3231. https://doi.org/10.1021/jf073304e

Tripathi, D.K., Shweta, Singh, Shweta, Singh, Swati, Pandey, R., Singh, V.P., Sharma, N.C., Prasad, S.M., Dubey, N.K., Chauhan, D.K., 2017. An overview on manufactured nanoparticles in plants: Uptake, translocation, accumulation and phytotoxicity. Plant Physiol. Biochem. 110, 2–12. https://doi.org/10.1016/j.plaphy.2016.07.030

Vatansever, R., Ozyigit, I.I., Filiz, E., 2017. Essential and Beneficial Trace Elements in Plants, and Their Transport in Roots: a Review. Appl. Biochem. Biotechnol. 181, 464–482. https://doi.org/10.1007/s12010-016-2224-3

Voegelin, A., Pfister, S., Scheinost, A.C., Marcus, M.A., Kretzschmar, R., 2005. Changes in Zinc Speciation in Field Soil after Contamination with Zinc Oxide. Environ. Sci. Technol. 39, 6616–6623. https://doi.org/10.1021/es047962g

Wang, L., Rinklebe, J., Tack, F.M.G., Hou, D., 2021. A review of green remediation strategies for heavy metal contaminated soil. Soil Use Manag. 37, 936–963. https://doi.org/https://doi.org/10.1111/sum.12717

Wang, P., Menzies, N.W., Lombi, E., McKenna, B.A., Johannessen, B., Glover, C.J., Kappen, P., Kopittke, P.M., 2013. Fate of ZnO Nanoparticles in Soils and Cowpea (*Vigna unguiculata*). Environ. Sci. Technol. 47, 13822–13830. https://doi.org/10.1021/es403466p

Webb, S.M., 2005. SIXpack: A graphical user interface for XAS analysis using IFEFFIT. Phys. Scr. T T115, 1011–1014. https://doi.org/10.1238/Physica.Topical.115a01011

Zaimoglu, Z., 2006. Treatment of campus wastewater by a pilot-scale constructed wetland utilizing *Typha latifolia*, *Juncus acutus* and *Iris versicolor*. J. Environ. Biol. 27, 293–298.

Zelano, I.O., Cloquet, C., van der Ent, A., Echevarria, G., Gley, R., Landrot, G., Pollastri, S., Fraysse, F., Montargès-Pelletier, E., 2020. Coupling nickel chemical speciation and isotope ratios to decipher nickel dynamics in the *Rinorea* cf. *bengalensis* -soil system in Malaysian Borneo. Plant Soil 454, 225–243. https://doi.org/10.1007/s11104-020-04541-0

Zeng, X.-W., Ma, L.Q., Qiu, R.-L., Tang, Y.-T., 2011. Effects of Zn on plant tolerance and non-protein thiol accumulation in Zn hyperaccumulator *Arabis paniculata* Franch. Environ. Exp. Bot. 70, 227–232. https://doi.org/10.1016/j.envexpbot.2010.09.009

Zhang, H., Zhao, F.-J., Sun, B., Davison, W., Mcgrath, S.P., 2001. A New Method to Measure Effective Soil Solution Concentration Predicts Copper Availability to Plants. Environ. Sci. Technol. 35, 2602–2607. https://doi.org/10.1021/es000268q

Zhao, F.-J., Moore, K.L., Lombi, E., Zhu, Y.-G., 2014. Imaging element distribution and speciation in plant cells. Trends Plant Sci. 19, 183–192. https://doi.org/https://doi.org/10.1016/j.tplants.2013.12.001

Zhou, L., Meng, Y., Vaghefi, S.A., Marras, P.A., Sui, C., Lu, C., Abbaspour, K.C., 2020. Uncertainty-based metal budget assessment at the watershed scale: Implications for environmental management practices. J. Hydrol. 584. https://doi.org/10.1016/j.jhydrol.2020.124699

Zoumis, T., Calmano, W., Förstner, U., 2000. Demobilization of Heavy Metals from Mine Waters. Acta Hydrochim. Hydrobiol. 28, 212–218. https://doi.org/10.1002/1521-401X(20004)28:4<212::AID-AHEH212>3.0.CO;2-U

Zovko, M., Romic, M., 2011. Soil Contamination by Trace Metals: Geochemical Behaviour as an Element of Risk Assessment, in: Dar, I.A. (Ed.), Earth and Environmental Sciences. InTech, pp. 437–456. https://doi.org/10.5772/25448

Captions

FIGURES

Figure 1. (a) Plantlet of *J. acutus* before the rhizobox experiment; (b) and (c) transplantation into the rhizoboxes (the black tubes are irrigation lines); (d) overview of the rhizoboxes (still uncovered by dark fabric). The red rectangles indicate the rhizoboxes with *J. acutus*. UCW (Unpolluted substrate Clean Water line), NCW (Naracauli, substrate Clean Water line), SMCW (Sa Masa substrate Clean Water line), UZnW (Unpolluted substrate Zn-spiked Water line), NCW (Naracauli, substrate Zn-spiked Water line), SMCW (Sa Masa substrate Zn-spiked Water line).

Figure 2. Plant growth during the experiment in the different substrates and irrigation lines. The error bars indicate the uncertainty calculated as $\frac{standard\ deviation(height\ measurements)}{\sqrt{number\ of\ measurements}}$. See Table 1 for sample acronyms.

Figure 3. The histograms allow comparing the Zn contents in substrates, rhizospheres, roots and stems of *J. acutus* for the Clean Water line (Zn_{water} 0.05 mg/l) (a) and the Zn-spiked Water line (Zn_{water} 180 mg/l) (b).

Figure 4. The histograms allow comparing BCF (biological concentration factor), BAC (biological accumulation factor) and TF (translocation factor) calculated for *J. acutus* plants for the Clean Water line (Zn_{water} 0.05 mg/l) (a) and the Zn-spiked Water line (Zn_{water} 180 mg/l) (b).

Figure 5. Zn K-edge (9.659 keV) XANES spectra of the substrates, rhizospheres and vegetal tissues (roots and stems) for the Clean Water line (Zn_{water} 0.05 mg/l) and the Zn-spiked Water line (Zn_{water} 180 mg/l), vertically shift for sake of comparison.

Figure 6. Results from the linear combination analysis of XANES for the substrates, rhizospheres and vegetal tissues (roots and stems) for the Clean Water line (Zn_{water} 0.05 mg/l) and the Zn-spiked Water line (Zn_{water} 180 mg/l). The sum of contribute fractions was fixed to 100%, the incertitude on the fraction values is around 8%.

855

856 TABLES

857 **Table 1. Name, acronym and description of the investigated samples.**

858 **Table 2. Results of XRD analysis performed on the substrates, rhizospheres and vegetal tissues (roots and stems). Quartz (Qtz),**
859 **phyllosilicates (Phyl), feldspars (Fs), dolomite (Dol), siderite (Sid), smithsonite (Smith), gypsum (Gy) hemimorphite (Hem),**
860 **cellulose (Cell). Smithsonite (Smith) and hemimorphite (Hem) are Zn containing mineral phases only revealed in Sa Masa**
861 **substrate and rhizospheres.**

862

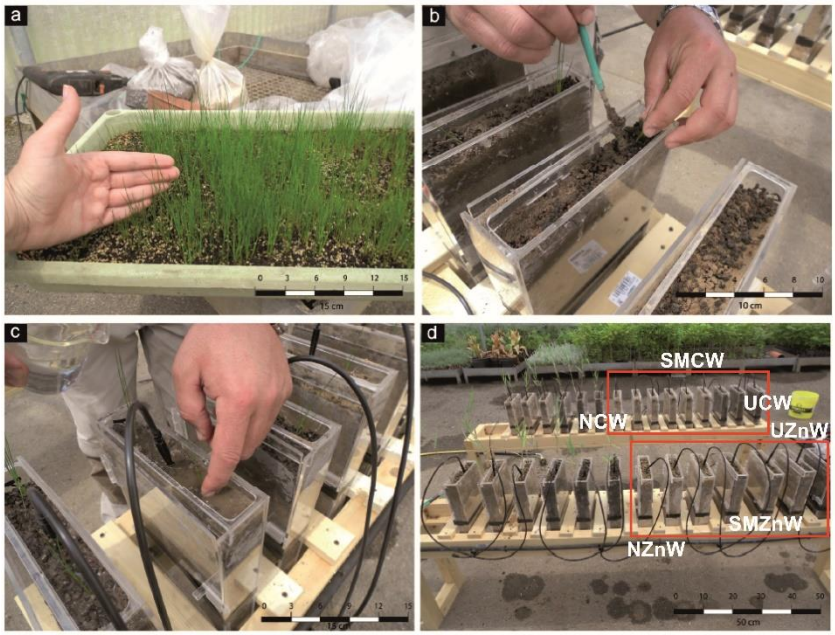

Figure 1. (a) Plantlet of *J. acutus* before the rhizobox experiment; (b) and (c) transplantation into the rhizoboxes (the black tubes are irrigation lines); (d) overview of the rhizoboxes (still uncovered by dark fabric). The red rectangles indicate the rhizoboxes with *J. acutus*. UCW (Unpolluted substrate Clean Water line), NCW (Naracauli, substrate Clean Water line), SMCW (Sa Masa substrate Clean Water line), UZnW (Unpolluted substrate Zn-spiked Water line), NCW (Naracauli, substrate Zn-spiked Water line), SMCW (Sa Masa substrate Zn-spiked Water line).

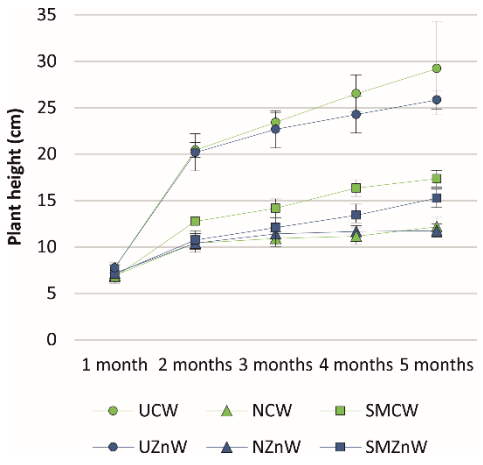

Figure 2. Plant growth during the experiment in the different substrates and irrigation lines. The error bars indicate the uncertainty calculated as $\frac{standard\ deviation(height\ measurements)}{\sqrt{number\ of\ measurements}}$. See Table 1 for sample acronyms.

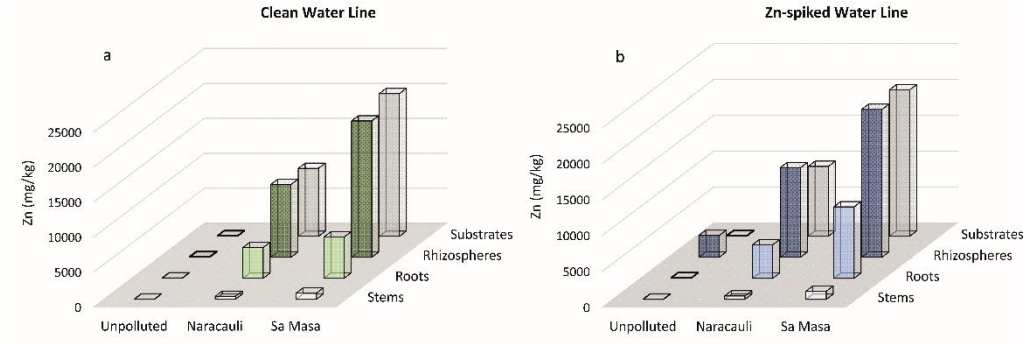

Figure 3. The histograms allow comparing the Zn contents in substrates, rhizospheres, roots and stems of *J. acutus* for the Clean Water line (Zn_{water} 0.05 mg/l) (a) and the Zn-spiked Water line (Zn_{water} 180 mg/l) (b).

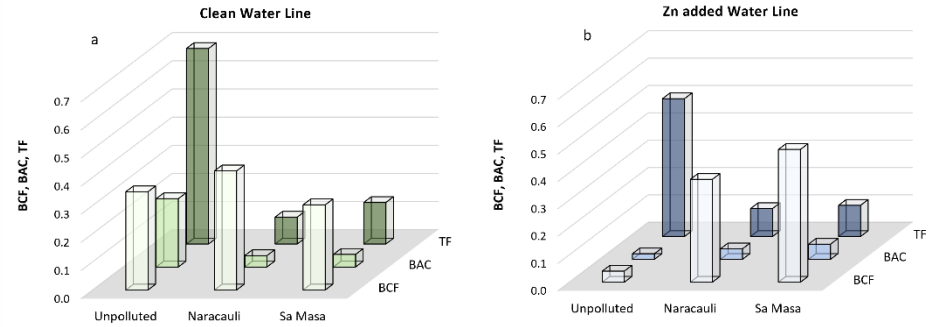

Figure 4. The histograms allow comparing BCF (biological concentration factor), BAC (biological accumulation factor) and TF (translocation factor) calculated for *J. acutus* plants for the Clean Water line (Zn_{water} 0.05 mg/l) (a) and the Zn-spiked Water line (Zn_{water} 180 mg/l) (b).

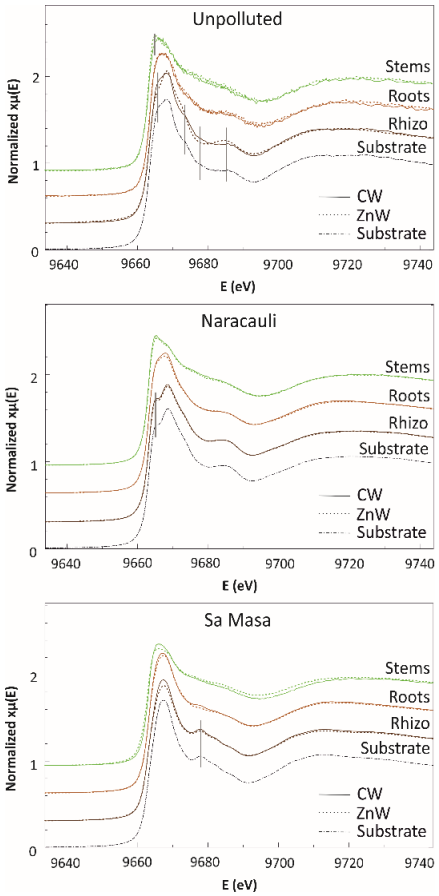

Figure 5. Zn K-edge (9.659 keV) XANES spectra of the substrates, rhizospheres and vegetal tissues (roots and stems) for the Clean Water line (Zn_{water} 0.05 mg/l) and the Zn-spiked Water line (Zn_{water} 180 mg/l), vertically shift for sake of comparison.

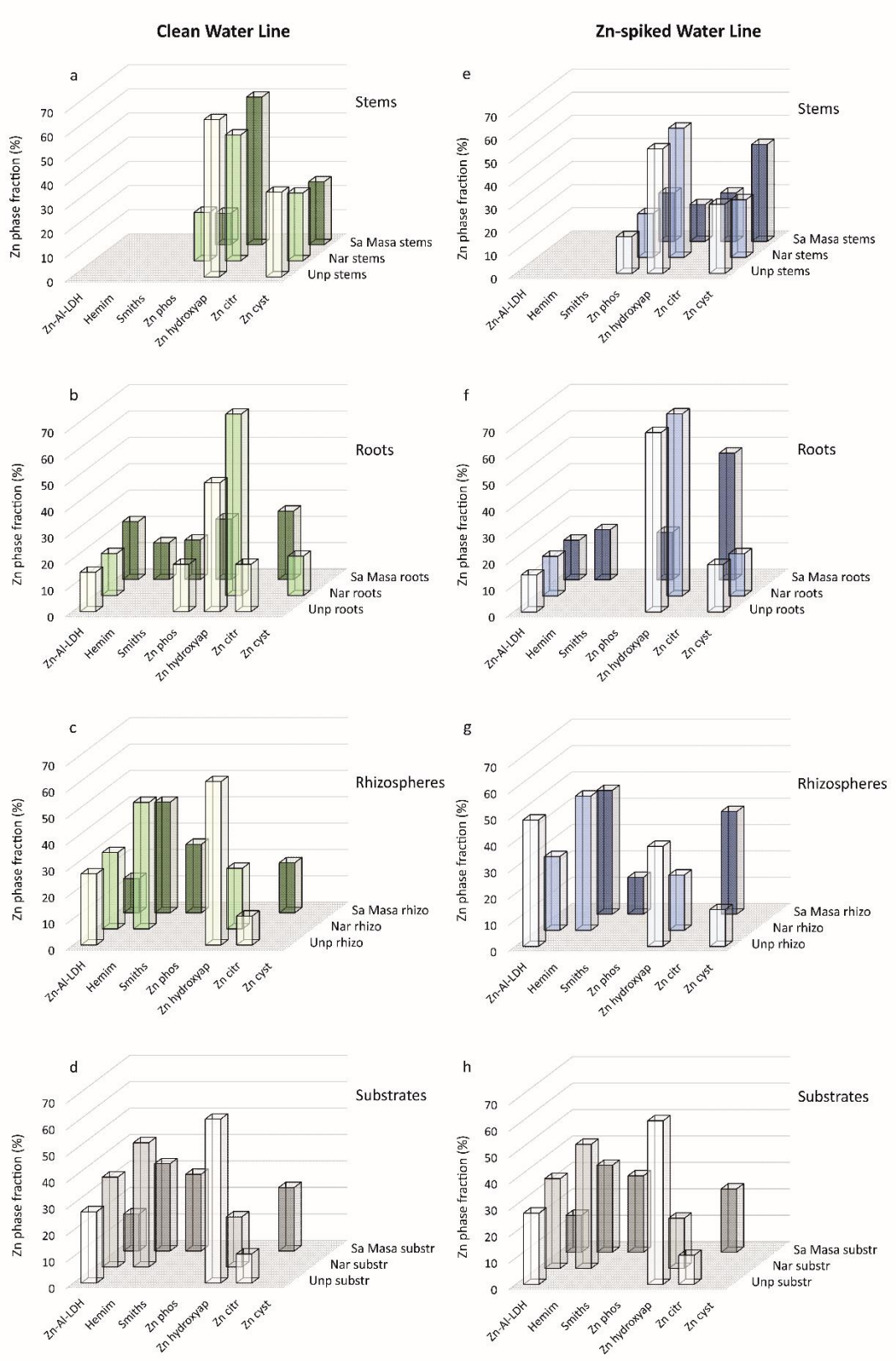

Figure 6. Results from the linear combination analysis of XANES for the substrates, rhizospheres and vegetal tissues (roots and stems) for the Clean Water line (Zn_{water} 0.05 mg/l) and the Zn-spiked Water line (Zn_{water} 180 mg/l). The sum of contribute fractions was fixed to 100%, the incertitude on the fraction values is around 8%.

Table 1. Name, acronym and description of the investigated samples.

Acronym	Sample		Description
-	Efflorescent salts		From the surface of the Naracauli and Sa Masa substrates (Clean Water line and Zn-spiked Water line)
U	Unpolluted substrate		Non polluted substrate (potting soils) before the rhizobox experiment.
N	Naracauli substrate		Mine wastes from the Naracauli area before the rhizobox experiment.
SM	Sa Masa substrate		Mine wastes from the Sa Masa pond before the rhizobox experiment.
CW			Clean Water line, (Zn_{water} 0.05 mg/l)
UCW	***Unpolluted system***		
UCW-rhizo		Rhizosphere	Rhizosphere collected at the end of the rhizobox experiment from the unpolluted group.
UCW-roots		Roots	Roots of *J. acutus* collected at the end of the rhizobox experiment from the unpolluted group.
UCW-stems		Stems	Stems of *J. acutus* collected at the end of the rhizobox experiment from the unpolluted group.
NCW	***Naracauli system***		
NCW-rhizo		Rhizosphere	Rhizosphere collected at the end of the rhizobox experiment from the Naracauli group.
NCW-roots		Roots	Roots of *J. acutus* collected at the end of the rhizobox experiment from the Naracauli group.
NCW-stems		Stems	Stems of *J. acutus* collected at the end of the rhizobox experiment from the Naracauli group.
SMCW	***Sa Masa system***		
SMCW-rhizo		Rhizosphere	Rhizosphere collected at the end of the rhizobox experiment from the Sa Masa group.
SMCW-roots		Roots	Roots of *J. acutus* collected at the end of the rhizobox experiment from the Sa Masa group.
SMCW-stems		Stems	Stems of *J. acutus* collected at the end of the rhizobox experiment from the Sa Masa group.
ZnW			Zn-spiked Water line, (Zn_{water} 180 mg/l)
UZnW	***Unpolluted system***		
UZnW-rhizo		Rhizosphere	Rhizosphere collected at the end of the rhizobox experiment from the unpolluted group.
UZnW-roots		Roots	Roots of *J. acutus* collected at the end of the rhizobox experiment from the unpolluted group.
UZnW-stems		Stems	Stems of *J. acutus* collected at the end of the rhizobox experiment from the unpolluted group.
NZnW	***Naracauli system***		
UZnW-rhizo		Rhizosphere	Rhizosphere collected at the end of the rhizobox experiment from the Naracauli group.
NZnW-roots		Roots	Roots of *J. acutus* collected at the end of the rhizobox experiment from the Naracauli group.
NZnW-stems		Stems	Stems of *J. acutus* collected at the end of the rhizobox experiment from the Naracauli group.
NZnW	***Sa Masa system***		
SMZnW-rhizo		Rhizosphere	Rhizosphere collected at the end of the rhizobox experiment from the Sa Masa group.
SMZnW-roots		Roots	Roots of *J. acutus* collected at the end of the rhizobox experiment from the Sa Masa group.
SMZnW-stems		Stems	Stems of *J. acutus* collected at the end of the rhizobox experiment from the Sa Masa group.

Table 2. Results of XRD analysis performed on the substrates, rhizospheres and vegetal tissues (roots and stems). Quartz (Qtz), phyllosilicates (Phyl), feldspars (Fs), dolomite (Dol), siderite (Sid), smithsonite (Smith), gypsum (Gy) hemimorphite (Hem), cellulose (Cell). Smithsonite (Smith) and hemimorphite (Hem) are Zn containing mineral phases only revealed in Sa Masa substrate and rhizospheres.

		Before the rhizobox experiment										Before the rhizobox experiment									
		Qtz	**Phyl**	**Fs**	**Cal**	**Dol**	**Sid**	**Smith**	**Gy**	**Hem**	**Cell**	**Qtz**	**Phyl**	**Fs**	**Cal**	**Dol**	**Sid**	**Smith**	**Gy**	**Hem**	**Cell**
Substrates	Unpolluted	x	x	x	x							x	x	x	x						
	Naracauli	x	x		x		x		x			x	x		x		x		x		
	Sa Masa	x			x	x		x		x		x			x	x		x		x	

		Clean Water line (Zn_{water} 0.05 mg/l)										Zn-spiked Water line (Zn_{water} 180 mg/l)									
		Qtz	**Phyl**	**Fs**	**Cal**	**Dol**	**Sid**	**Smith**	**Gyps**	**Hem**	**Cell**	**Qtz**	**Phyl**	**Fs**	**Cal**	**Dol**	**Sid**	**Smith**	**Gyps**	**Hem**	**Cell**
Rhizosphere	Unpolluted	x	x	x	x							x	x	x	x						
	Naracauli	x	x		x		x		x			x	x		x		x		x		
	Sa Masa	x			x	x		x		x		x			x	x		x		x	
Roots	Unpolluted	x			x						x	x			x						x
	Naracauli	x									x	x									x
	Sa Masa	x			x	x					x	x			x	x					x
Stems	Unpolluted										x										x
	Naracauli										x										x
	Sa Masa										x										x

- Metals released into the environment will inevitably interact with plants
- *J. Acutus* was exposed to different Zn sources (rhizosphere minerals and water)
- Zn accumulation and distribution changed differently in the investigated systems
- Zn detoxification was driven by variations in its speciation
- Rhizosphere minerals play a critical role in metal complexation by *J. acutus*